Dentate neurogenesis mediates cognitive flexibility via modulation of the hippocampal longitudinal-axis network

Haowei Li[1], Risako Tamura[1], Daiki Hayashi[1], Hirotaka Asai[1], Junya Koga[1], Shota Ando[1], Sayumi Yokota[1], Jun Kaneko[1], Keisuke Sakurai[1], Akira Sumiyoshi[2], Tadashi Yamamoto[3], Keigo Hikishima[3], Kazumasa Z. Tanaka[3,4], Thomas J. McHugh[4], Tatsuhiro Hisatsune[1*]

[1]Department of Integrated Biosciences, Graduate School of Frontier Sciences, The University of Tokyo, Kashiwa, Japan
[2]Department of Molecular Imaging and Theranostics, National Institutes for Quantum and Radiological Science and Technology (QST), Chiba, Japan
[3]Okinawa Institute of Science and Technology Graduate University, Okinawa, Japan
[4]Laboratory for Circuit and Behavioral Physiology, RIKEN Center for Brain Science, Saitama, Japan

Highlights:

- A new transgenic mouse model for non-invasive newborn neuron silencing.
- Newborn neuron silencing imbalances dentate gyrus excitation and inhibition.
- Deficits in young newborn neuron alters hippocampal longitudinal activation.
- Hyperactivated hippocampus hinder its dorsal-ventral functional separation.
- Hippocampal longitudinal networks maintain cognitive flexibility.

Summary

Adult neurogenesis provides the hippocampus with significant neuroplasticity, supporting its involvement in complex functions, including cognitive flexibility. However, it remains unclear how these relatively sparse newborn neurons (NBNs) affect brain activity and regulate behavior. In this study, we silenced young NBNs (2-5 weeks old) non-invasively in a newly generated transgenic mouse model (NBN-TeTX) in which tetanus toxin is expressed in NBNs and confirmed their contribution to cognitive flexibility using the Morris water maze reversal learning and an operant learning Go/NoGo task. fMRI during the NoGo task revealed altered activity across the hippocampal longitudinal networks in the NBN-TeTX mice, while resting-state fMRI indicated that NBNs also contributed to inverse dorso-ventral inter-hippocampal correlations. Further investigation of the dentate gyrus excitation-inhibition circuits revealed that silencing young NBNs reduced parvalbumin (PV) expression in inhibitory basket cells but increased c-Fos expression in excitatory mossy cells, suggesting that NBNs contribute to local signal-to-noise ratio maintenance. This plasticity in the hippocampal longitudinal-axis network mediated by young NBNs may contribute to cognitive flexibility.

Keywords: neurogenesis, hippocampus, cognitive flexibility, inhibitory control, reversal learning, fMRI, functional heterogeneity, functional connectivity.

Introduction

Organized memories enable individuals to behave appropriately in complex situations while avoiding the cognitive overload of neural circuits (Anderson and Hanslmayr, 2014; Ryan and Frankland, 2022). This balance is heavily reliant on executive functions, which consist primarily of working memory, inhibitory control, and cognitive flexibility (Collins and Koechlin, 2012; Diamond, 2013; Miyake et al., 2000), and the hippocampus is intimately involved as a key site for the execution of higher cognitive functions such as learning and memory(Squire, 1992; Voss et al., 2017). It is now widely accepted that neuroplasticity is the primary neural mechanism underlying the hippocampus's role as a learning-memory center (Maletic-Savatic et al., 1999; Matsuzaki et al., 2004), and that this neuroplasticity spans multiple scales and dimensions, including dendritic plasticity, axonal plasticity, synaptic plasticity, and neural circuit plasticity. Simultaneously, the hippocampus's capacity for adult neurogenesis not only endows it with additional mechanisms of neuroplasticity, but also provides a new perspective for further revealing its own function.

Current evidence suggests that continuous neurogenesis occurs in both animals and humans within the hippocampal dentate gyrus (Kempermann, 2015; Taupin and Gage, 2002). Until five weeks after birth, these newborn neurons (NBNs) exhibit unique physiological properties such as hyperexcitability and high plasticity (Ge et al., 2007), allowing them to recruit inhibitory GABAergic interneurons and act as inhibitors of mature granule cell activity in the dentate gyrus (Drew et al., 2016; Ikrar et al., 2013). Numerous studies have confirmed the role of immature NBNs in novelty encoding, fear memory extinction (Denny et al., 2012; Huckleberry et al., 2018), and spatiotemporal information processing (Aimone et al., 2006; Dupret et al., 2008) during hippocampus-dependent cognition. Higher cognitive functions such as pattern separation and reversal learning have also been shown to benefit from the continuous integration of NBNs into existing neural circuits (Burghardt et al., 2012; Toni and Schinder, 2016). Moreover, the reconfiguration of neural networks caused by the insertion of new neurons may destabilize previous memory circuits, facilitating some forms of forgetting (Chen et al., 2022; Yau et al., 2015), providing the foundations for cognitive flexibility. However, there is limited observations (Epp et al., 2016) and theoretical hypotheses (Aimone et al., 2009) which limit not only the discovery of NBNs' functions, but also their interaction with the entire brain. With an increased understanding of hippocampal functional heterogeneity along the longitudinal axis (Fanselow and Dong, 2010; Strange et al., 2014b) and the physiological effects of emotion and stress on NBNs (Anacker and Hen, 2017; O'Leary and Cryan, 2014), previous assessments of the existence and functional significance of NBNs may need to be revised. In addition, data on the contribution of NBNs to local circuit excitation/inhibition balance (Sun et al., 2009) are incomplete under normal physiological condition. Therefore, a challenging question is how to visualize the contribution of NBNs to brain networks in a physiological setting that is as natural as possible to describe their function, action period, and influence.

Here we report the generation of a new transgenic mouse (NBN-TeTX) (Imayoshi et al., 2006; Imayoshi et al., 2008; Nakashiba et al., 2012; Nakashiba et al., 2008), capable of noninvasively silencing the function of NBNs. Through multiple reversal learning tasks (Epp et al., 2016; Sakurai et al., 2020), we confirmed impairments in inhibitory control and cognitive flexibility induced by silencing young NBNs (2-5 weeks old). In addition, fMRI allowed us to visualize the longitudinal activation pattern of the hippocampus during the task state (Dinh et al., 2021; Han et

al., 2019). By examining the phenotypes of GABAergic interneurons and excitatory mossy cells in the dentate gyrus (Ide et al., 2008; Toni et al., 2008), we hypothesize that NBNs support cognitive flexibility through regulating the signal-to-noise ratio across the longitudinal-axis circuit at the dentate gyrus. Our fMRI data provide a practical foundation for observing the effects of NBNs on brain activity. In addition, the abnormal activation patterns and functional connectivity alterations detected by fMRI provide evidence and a roadmap for further elucidating the contribution of the hippocampus and NBNs to spatiotemporal perception and cognitive flexibility.

Results

Tetanus toxin (TeTX) expression in newborn neurons inhibits both neurotransmitter release and survival

The genetic composition of the triple transgenic NBN-TeTX mice (Tg) and the mechanism of silencing NBNs is illustrated in **Fig. 1a**. Tamoxifen injection specifically induces TeTX expression in the newborn neurons of mice carrying all three recombinant genes, resulting in the blockade of synaptic vesicle release via the TeTX-mediated cleavage of vesicle-associated membrane protein 2 (VAMP2) (**Fig. 1a**). A viral-mediated approach ((**Fig. 1b, also see methods**) to label both synaptic vesicles (GFP) and VAMP2 (mCherry) confirmed that TeTX expression in NBN synaptic terminals in CA3 lead to a roughly 40% reduction in VAMP2 containing vesicles in the mutant mice compared to controls (**Fig. 1c**), suggesting a significant loss of synaptic transmission. Further, contrary to our hypothesis that TeTX expression in NBN would prevent the release of neurotransmitters without affecting the survival of newborn neurons, BrdU injections, which labels newly post-mitotic neurons, revealed a significant decrease in the number of NBNs in the dentate gyrus (subgranular zone). Eight weeks after Tamoxifen/BrdU injections, the number of newborn neurons in NBN-TeTX was significantly lower than in the control group (**Fig. 1d**).

We next further investigated the stage at which TeTX expression impacted the survival of newborn neurons by crossing a fourth transgenic allele, tetO-EYFP, into the NBN-TeTX genetic background to label surviving TeTX neurons with EYFP (**Fig. 2a-c**). Four weeks after Tamoxifen/BrdU injections the number of EYFP-positive cells that survived in NBN-TeTX-EYFP mice was significantly lower than in the control ($p < 0.001$; **Fig. 2d**). Consistent with this, the number of NeuN+/BrdU+ neurons that were also positive for DCX, a marker for immature cells, suggested that the survival rate of NBNs in these mice was approximately 50% (**Fig. 2e**).
DCX+ cells can be subdivided into NeuN-positive (DCX+/NeuN+) and NeuN-negative cells (DCX+/NeuN-) subpopulations. DCX+/NeuN- cells are progenitor cells that have not yet differentiated into neurons, whereas DCX+/NeuN+ cells are indicative of immature NBNs. Two weeks after tamoxifen injection, NBN-TeTX mice began to exhibit a trend towards the reduction in the number of DCX+/NeuN+ immature newborn neurons. Four weeks later (**Fig. 2f**), we detected a significant decrease in the number of DCX+/NeuN+, but not DCX+/NeuN- cells, in the NBN-TeTX mice, suggesting that TeTX expressions in developing NBNs that have already expressed CAMKII reduces the survival of immature NBNs approximately two weeks after the final neuronal differentiation. Therefore, NBN-TeTX mice provide a unique experimental tool, as the NBN-specific transgenic expression of TeTX reduces the survival of young NBNs to 50%, while the remaining function of NBNs is significantly inhibited by TeTX expression.

Silencing NBNs impedes spatial reversal learning

To probe the effects of NBN TeTX expression on cognitive flexibility, we conducted the Morris water maze experiment with a reversal learning paradigm. 13 NBN-TeTX mice (Tg) and 11 control mice (Ctrl) were exposed to 5 days of acquisition learning (D1-D5), followed by 5 days of reversal learning (D6-D10). Three spatial probe examinations were scheduled for day 5 (after acquisition learning), day 10 (after reversal learning), and day 13 accordingly **(Fig. 3a)**. Across the 10-day training period there were no significant differences in swimming speed and total swimming distance between the two groups. As shown in **Fig. 3b** (D1-D5), there was no significant difference between the Tg and Ctrl groups during the first 5 days of acquisition learning and in the first spatial probe test (P1) performed immediately after the final day of acquisition learning (D5), the results revealed no significant differences in the duration of stay in the target quadrant (NE), thus silencing NBNs did not interfere with the initial spatial learning.

During reversal learning (D6-D10), the platform shifted from the NE to the SW quadrant and as seen in **Fig. 3b**, the Tg group exhibited an escape latency that significantly lagged behind that of the control group ($p < 0.05$), with no different in swim speed between the groups (**Fig. 3c**). In the second spatial probe test (P2) conducted immediately after the final day of reversal learning (D10), the preference for regions differed between the two groups, with Ctrl mice exploring the platform's new location (SW), whereas the Tg group tended to explore the platform's original location (NE) (**Fig. 3d**). The third spatial probe test (P3) was conducted on day 13 to examine the final long-term memory formed in both groups after 10-days of combined initial and reversal learning. At this time point the Ctrl mice spent equal time exploring both previous goal locations (NE and SW zones), whereas the Tg group still showed a clear preference for the NE **(Fig. 3d**, P3**)**. In summary, these data suggest that the NBN-TeTX mice's initially formed memories were consolidated and determined their future behavior, preventing the establishment of an update memory during the reversal phase.

Silencing NBNs reduces reversal learning in an operant Go/NoGo task.

To examine cognitive flexibility in the NBN-TeTX mice further, we devised an operant learning Go and NoGo task to evaluate reinforcement learning as well as inhibitory control (behavioral inhibition), one component of cognitive flexibility in mice (**Fig. 4a**). We trained 11 NBN-TeTX mice (Tg) and 9 control mice on a 10-day "Go task" in which they learned that licking in response to light stimulation ("Cue") led to a water reward ("Reward"). The data revealed that the percentage of correct responses (Correct%) increased gradually over the course of 10 days and remained around 95% by the end of the training in both the NBN-TeTX and Ctrl groups (**Fig. 4b**). During D11-D20, we switched the operant learning task to a NoGo Task, in which mice were required to inhibit their learned water-licking response in response to the onset of the light cue and wait until the light ended to receive a water reward. As shown in **Fig. 4c**, the Tg group exhibited a consistent deficit in inhibiting their licking response throughout the 10-day experiment, resulting in a significant decrease in correct responses compared to the control group. This suggests that silencing NBNs impaired inhibitory control (behavioral inhibition) in NBN-TeTX mice, causing them to exhibit compulsive behavior heavily reliant on their initial memory.

NBN-TeTX mice exhibit hyperactivation of dorsal hippocampus during reversal learning.

To visualize the functional role of NBNs in the context of the longitudinal hippocampal circuit, we combined awake task-based fMRI (tb-fMRI) with the reversal learning task described above. In awake mice we were able to observe the real-time activity of the entire brain during task performance. 6 NBN-TeTX and 6 control mice were place into the MRI and first completed 3 days of water licking training and 3 days of the Go task following a procedure similar to that previously described for operant-learning, during which the number of licks per day, the number of incorrect licks, and the response time were evaluated for each group to ensure the same level of learning and behavioral performance (**Fig. 5a**). On day 7, a 3-minute NoGo task was performed immediately after. However, this time we required the mice to actively lick just after cue termination to be considered correct and rewarded with water. This rule is intended to eliminate the possibility of mice receiving water rewards directly due to inaction caused by factors such as the relative cold within the MRI and the noise during scanning, allowing for a more precise evaluation of brain activity and behavior in the reversal learning task. In the nine NoGo task trials during the formal fMRI scan, the correct rate of water reward by inhibiting licking for each group is shown in **Figure 5c**, with the NBN-TeTX group again demonstrating a significantly lower success rate compared to the Ctrl group. We used a hippocampal mask (**Fig. 5b, mark 4**) during the tb-fMRI analysis to focus on changes of activity in the hippocampus.

The percentage changes in the hippocampal BOLD signal during NoGo tb-fMRI scans were measured in both groups **(Fig. 5d)** and the mean BOLD signal intensity was extracted from functional images of each mouse at each time point to plot the dynamics of hippocampal activity. We observed that, relative to the baseline level (the mean BOLD value in the last 4s within each trail), the mean %BOLD signal intensity in the hippocampus was increased in both groups of mice within 4-6s after light stimulation, but the mean %BOLD increment in the Tg group was approximately 2.45 times greater than that in the control (**Fig. 5d**, $p<0.05$). In the first-level individual analysis, we noticed that Tg individuals had generally higher hippocampal activation patterns than Ctrl subjects (**Fig. 5f**, show representative individuals).

We further confirmed the distinction in hippocampal activation patterns between the Tg group and the Ctrl group with a second-level intragroup analysis (**Fig. 6a**), again revealing abnormally hippocampal hyperactivity patterns caused by silencing NBNs. Notably, the majority of these abnormal hyperactivations were located near the dentate gyrus in the dorsal hippocampus, whereas ventral hippocampus activity was relatively unchanged (**Fig. 6d**). To determine whether this abnormal activation differed across the dorsoventral axis, we divided the hippocampus into ten equal parts horizontally along the longitudinal axis (**Fig. 6e**). The top five segments were considered to be the dorsal hippocampus (d1-d5), the middle two segments were considered to be the middle (M), and the bottom three segments were considered to be the ventral hippocampus (v1-v3). Using the same parameters as in the previous analysis, we compared the increase in percent BOLD signal change in each segment of the activated hippocampus to the level at baseline. The results confirmed that abnormal hyperactivation in NBN-TeTX mice was prominently localized in the most dorsal region (d1-d3) and gradually decreased along the longitudinal axis (d4-d5) (**Fig. 6b, c**). This significant difference between groups persisted until the middle segments and was synchronized in both the left and right hippocampus. In summary, fMRI visualized the region and magnitude of the NBNs' effect on hippocampal activity, confirming that silent NBNs induce abnormally high hippocampal hyperactivation during

hippocampus-dependent reversal learning.

Silencing NBNs causes abnormal enhancement of functional connectivity between the dorsal and ventral dentate gyrus.

To identify potential triggers for the hyperactivation pattern of the task-state hippocampus exhibiting dorsoventral segregation following NBN silencing, we performed functional connectivity (FC) analysis in resting-state mice based on hippocampal structural compositions, dividing the bilateral hippocampus into 6 regions of interest (ROIs) anatomically and dorsoventrally (**Fig. 7b**). Six minutes of fMRI data were collected in 14 NBN-TeTX (Tg) and 14 control mice (Ctrl). The functional connectivity connectome ring between regions in the Tg and Ctrl groups were generally similar in the 2nd-level intragroup analysis, but there were still distinct differences between both dDG-vDG and dCA2&3-vCA2&3 groups (**Fig. 7a**). The comparison of functional connectivity effect sizes and trends of alteration among the entire regions between NBN-TeTX group and Ctrl group are presented in **Figure 7c**., while dDG-vDG survived the Tg-Ctrl intergroup analysis under p=0.016, with the Tg group presenting a significantly diminished negative correlation compared to the Ctrl group. In summary, functional connectivity analysis confirmed the abnormal correlation coefficient enhancement between the dorsal and ventral dentate gyrus deriving from silent NBNs. This alteration may underlie the altered hippocampal activation pattern that we observed in the task state.

Unbalanced dentate gyrus local excitation-inhibition following NBN silencing.

Our previous results indicate that silent NBNs cause abnormal hyperactivation within the hippocampus, as well as enhanced functional connectivity between the dorsal and ventral dentate gyrus. To investigate the possible mechanisms underlying this, we examined the number of GABAergic interneurons and mossy cells, which are major components of the DG local excitatory-inhibitory circuits, three weeks after tamoxifen injection. We counted parvalbumin cells (PV+, GABAergic interneurons) and GluR2/3+ cells (mossy cells) by immunofluorescence staining in the hippocampus of Tg and control mice that were not subjected to behavioral experiments. Taking into account the functional heterogeneity exhibited by the hippocampus along the longitudinal axis, we conducted separate counts in coronal and axial slices, respectively. Similar to the segmentation used for tb-fMRI, the hippocampus was divided into dorsal, middle, and ventral regions for axial slice counting.

Coronal slice staining revealed that in NBN-TeTX mice, the number of PV+ neurons was significantly reduced in both the dorsal and ventral DG. However, neither the number nor the fluorescence intensity of mossy cells represented by GluR2/3 staining changed significantly in the hilar region (**Fig. 8b**). The axial section results supported this, with significantly fewer PV+ cells in the Tg group observed in the dorsal, middle, and ventral hippocampus, while the number of mossy cells did not differ significantly (**Fig. 8c**). Notably, the decrease in the number of PV+ neurons did not vary between the dorsal and ventral hippocampus. Although there was no change in the number of GluR2/3 + mossy cells, co-staining with an antibody for c-Fos, an immediate early gene marker for neuronal activity (Sagar et al., 1988) revealed significant and consistent differences in both coronal and axial sections. The Tg group had significantly more GluR2/3+/c-Fos+ cells than the Ctrl group, and the changes were consistent between the dorsal and ventral

regions of the hippocampus (**Fig. 8d**). Notably, when we examined the number of DCX+/NeuN+ cells representing immature neurons again using the same method, we found a simultaneous dorsal-ventral difference in both groups, with the total number of newborn neurons higher dorsally than ventrally (**Fig. 8a**).

To compare the relative ratio of the main excitatory/inhibitory circuit components in the DG, we divided the number of PV-expressing inhibitory interneurons by the number of GluR2/3 and c-Fos double positive excitatory mossy cells, observing that the inhibitory components was higher than excitatory components in the Ctrl group, with the inhibition coefficient being higher dorsally. In contrast, the inhibitory coefficient was dramatically reduced in the NBN-TeTX group. Furthermore, the inhibitory advantage of the dorsal side compared to the ventral vanished after newborn neuron silencing (**Fig. 8e**).

In summary, silencing NBNs reduced the number of PV+ neurons in the local excitatory-inhibitory circuits of the dentate gyrus while simultaneously increasing the activity of GluR2/3-labeled mossy cells. Simultaneously, silencing newborn neurons resulted in a greater loss of the dentate gyrus inhibitory coefficient dorsally compared to ventrally.

Discussion

Non-invasive silencing NBNs in new triple transgenic mouse NBN-TeTX.

Adult hippocampal neurogenesis is widespread in mammals, including humans (Ming and Song, 2011; Spalding et al., 2013), but the significance of the existence and function of NBNs is still debated due to limited modulation and observational methods. However, it is undeniable that the unique contribution of NBNs to individual cognitive abilities and behavioral regulation is far more impressive than their sparse numbers. Previous studies of NBNs' function have demonstrated the contribution of NBNs to novelty encoding, spatial navigation, and learning (Toda et al., 2019; Zhao et al., 2008) by increasing the number of NBNs under environmental enrichment (Kempermann et al., 1997) and destroying newborn granule cell populations through X-irradiation (Burghardt et al., 2012; Lacefield et al., 2012). However, the description of their functions has not always been consistent (Ambrogini et al., 2004; Dupret et al., 2007b). Therefore, to further reveal the function of NBN a non-invasive method for modulating the number of NBNs without disrupting the hippocampal anatomy was desired. To that end, we combined two transgenic systems in this study. In Nes-CreERT2 transgenic mice, neural stem/progenitor cells at the desired time point could be permanently labeled after tamoxifen administration (Imayoshi et al., 2006). In contrast, in TeTX transgenic mice, tetanus toxin is expressed under the control of the CamKII promoter and tetracycline trans-activation, in which the application of the doxycycline inhibited the expression of tetanus toxin, enabling inducible and reversible inhibition of synaptic transmission (Nakashiba et al., 2008). By fusing these two properties, we generated the NBN-TeTX mouse model, making it possible to non-invasively silence NBNs and restore their function at specific times as needed.

In this study, we also observed that the survival of NBN was affected by the expression of TeTX (**Fig. 2**). NBNs develop from neural stem/progenitor cells through DCX+/NeuN- type3 progenitor cells (Toda et al., 2019; Tozuka et al., 2005). The survival of DCX+/NeuN- cells was

unaffected in NBN-TeTX mice, however the survival of post-mitotic DCX+/NeuN+ young NBN was substantially decreased. The cell death of young NBN has been repeatedly reported in various experimental settings (Dupret et al., 2007a; Pilz et al., 2018; Tashiro et al., 2007). DCX+ young NBNs range in age from 1 to 3 weeks and exhibit neuronal excitation as action potential (Heigele et al., 2016). Young NBNs receive excitatory GABAergic inputs from the progenitor cell stage (Ge et al., 2006; Tozuka et al., 2005) and extend their axons toward GABAergic interneurons as well as excitatory mossy cells at the hilar region after 7 days of birth (Heigele et al., 2016; Ide et al., 2008). Therefore, young NBNs are incorporated into the neural circuit at the hilar region of the dentate gyrus and may contribute to the regulation of local excitatory/inhibitory balance. The lack of synaptic transmission that is sensitive to TeTX expression may affect the survival of young NBN. In addition, recent studies suggest additional actions of tetanus toxin, as tetanus toxin can cleave VAMP1 and VAMP3 molecules in addition to VAMP2 (Ferecsko et al., 2015; Luftman et al., 2009; Yamamoto et al., 2003). VAMP2 and VAMP1 are normally involved in the release of neurotransmitters, while in contrast, VAMP3 is recruited into endosomes and autophagosomes (Puri et al., 2013; Wu et al., 2016). The block of autophagy in developing neurons by ATG5 or ATG7 conditional knock-out using Nestin-Cre mice cause neurodegenerations (Hara et al., 2006; Komatsu et al., 2006). VAMP3 plays an important role in the formation of autophagosomes, suggesting these cellular events may also be essential to maintain the survival of young NBN. Further studies are needed to elucidate the effect of tetanus toxin expression in young NBN in the context of inducing cell death, but nonetheless, the NBN-TeTX mice cause a non-invasive silencing of NBN by reducing the number of surviving NBN as well as blocking neurotransmitter release, which offers a unique transgenic tool to analyze the role of NBN in network as well as cognitive functions.

Contribution of NBNs to the hippocampal longitudinal-axis network.

The dentate gyrus is involved in hippocampal-dependent learning and memory, with pattern separation being the most frequently cited process (Hainmueller and Bartos, 2020; Leutgeb et al., 2007; McHugh et al., 2007). Both neurogenesis ablation and optogenetic silencing experiments have demonstrated the contribution of NBNs to discriminating between highly similar environments (Clelland et al., 2009; Creer et al., 2010). However, discrete coding of similar information is the foundation for pattern separation, so sparse activity patterns in the dentate gyrus should be required (McAvoy et al., 2015), and the high excitability of NBNs at specific times may temporarily support this sparse hippocampal population activity compared to mature dentate granule cells (McHugh et al., 2022). We also propose that young newborn neurons may influence the hippocampal longitudinal-axis network through regulating the dentate gyrus excitation/inhibition balance.

Humans fMRI analysis has been widely used to investigate the longitudinal function of the hippocampus with fruitful results (Poppenk et al., 2013; Small et al., 2001). It is generally accepted that the posterior (dorsal) hippocampus is mainly used for spatial memory and the anterior (ventral) hippocampus for emotional control, but there is a contradictory theory that both regions are necessary, and a complete conclusion has not been reached (Strange et al., 2014a). Therefore, a unified understanding of which part of the hippocampus is responsible for cognitive flexibility (inhibition and reversal learning), which is the subject of this study, has not yet been achieved even in humans. In a rodent model study, the connection between the ventral hippocampus and the frontal lobe was proposed to be important, and indeed, an fMRI analysis of the activity of this region during the implementation of reversal learning has been awaited. To

achieve this goal, we and others have been working on establishing an experimental system to collect fMRI data from mice performing the Go/NoGo task (Han et al., 2019; Sakurai et al., 2020), and in this paper, we succeeded in imaging hippocampal activity from mice performing the NoGo task. We found that the activity of the dorsal hippocampus was elevated during the NoGo task, and this dorsal hippocampal activity was hyperactivated in NBN-TeTX mice. In addition, resting-state fMRI also indicated an alteration of the functional connectivity between the dorsal and ventral dentate gyrus in NBN-TeTX. These findings suggest that NBN contributes to maintaining the hippocampal longitudinal network by regulating local excitatory/inhibitory balance.

Based on the fact that fMRI analysis revealed abnormally elevated local activity in the hippocampal dentate gyrus of NBN-TeTX mice, we examined the major components of the dentate gyrus' excitation/inhibition circuits. Granule cells, GABAergic interneurons, and mossy cells make up the majority of the dentate gyrus' cell types (Amaral et al., 2007). The calcium-binding protein parvalbumin (PV) is generally employed to mark these basket cells, and PV+ interneurons have a dense dendritic structure and can form broad synaptic connections with excitatory cells at various levels. By fully receiving excitatory impulses, detecting excitation levels, and uniformly transmitting inhibitory signals to surrounding neurons, they delicately maintain the excitation/inhibition balance of neural circuits (Dieni et al., 2013; Ide et al., 2008). Mossy cells in the hippocampal hilus, as the major excitatory neurons, are thought to be sentinels of the DG network (Scharfman, 2016). Their axons in the ipsilateral extension (commissural pathway) span approximately sixty percent of the DG's longitudinal axis (Scharfman and Myers, 2012). Extensive projections enable mossy cells to regulate the excitation/inhibition homeostasis of granule cells within the DG (Hsu et al., 2016; Scharfman, 1995). Very interestingly, ventral mossy cells communicate with the dendrites of PV+ interneurons so infrequently that they do not exert much excitatory action on dorsal granule cells (Fredes et al., 2021). However, the inconsistency of neurogenesis levels dorsoventrally is likely to introduce uncertainty into the typical longitudinal regulatory circuits following the loss of newborn neurons for some reason. In conclusion, while we have not been able to determine the sequence or specific mechanism of the downregulation of PV+ interneuron numbers and the increase in mossy cell activity as a result of newborn neuron silencing, it is undeniable that NBNs play an important role in regulating the delicate dentate gyrus's local excitation/inhibition balance (**Fig. 8e**).

NBNs and hippocampal longitudinal-axis network contribute to cognitive flexibility.

Our findings clearly show that hippocampal neurogenesis contributes to maintaining cognitive flexibility, as evidenced by reversal learning and behavioral inhibition. A working hypothesis holds that cognitive flexibility necessitates close cooperation between working memory and inhibitory control. In addition to the prefrontal cortex (PFC), it is now understood that the hippocampus is also closely involved in the realization of cognitive flexibility (Burghardt et al., 2012; Garthe et al., 2009; Monk et al., 2002), for instance by participating in reversal learning (Swan et al., 2014). In this study, we tested reversal learning based on MWM and operant-learning, which included contextual switching, spatial orientation, and conditioning change. The findings clearly demonstrated that NBNs participate in reversal learning, implying that NBNs are required for cognitive flexibility. Moreover, our imaging results suggest that in addition to other non-invasive brain imaging methods developed previously, the fMRI method for measuring hippocampal activity along the longitudinal axis during reversal learning may be one of the most effective methods for assessing the state of hippocampal neurogenesis, even in humans. Through

incorporation into the neural network of the hippocampal dentate gyrus and maintenance of the longitudinal-axis hippocampal network, the current study demonstrates that even young NBNs can contribute to the execution of cognitive flexibility.

Conclusion

In this study, 2-5-week-old young newborn neurons (NBNs) were silenced non-invasively using a newly constructed NBN-TeTX mouse. We confirmed the contribution of NBNs to cognitive flexibility by employing behavioral experiments involving reversal learning. As essential components of dentate gyrus homeostasis, the dysfunction of GABAergic interneurons and increased mossy cell activity following newborn neuron silencing lead to dysregulation of local inhibitory circuits, resulting in diminished functional antagonism of the dorsoventral dentate gyrus, which may ultimately contribute to cognitive dysfunction.

Methods

Transgenic composition of NBNs-TeTX mice

The three recombinant genes, Tg1, Tg2, and Tg3, are described as follows: Tg1 expresses Cre/ERT2 protein downstream of the Nestin promoter (Nestin-Cre/ERT2), an intermediate filament specifically expressed in neural stem and progenitor cells. Tg2 contains two loxP sequences downstream of the αCamKII promoter and a recombinant gene with a stop codon between them. It is specifically active in forebrain neurons and expresses tTA (tetracycline transactivator) downstream of it (αCamKII-loxP-STOP-loxP-tTA). Tg3 expresses tetanus toxin downstream of TetO (Tetracycline Operator) (TeTX) recombinant gene (TetO-TeTX).

In NBN-TeTX mice with the above three types of recombinant genes, TeTX expression can be induced specifically by tamoxifen injection, which inhibits the function of NBNs. When tamoxifen is administered, the metabolite of tamoxifen, 4-OHT (estrogen analogue), binds to ERT, allowing Cre/ERT2 to enter the nucleus and exert Cre recombinase activity in Nestin-positive neural stem/progenitor cells. Its action on the loxP of Tg2 leads to removing the STOP codon in Tg2. When these neural stem/progenitor cells with STOP codons are removed from Tg2 due to Cre recombinase activity differentiate into neurons, the downstream αCamKII promoter is activated and expresses tTA (tetracycline controlled transcriptional activator). Subsequently, tTA binds to TetO of Tg3 and initiates its downstream transcription, leading to the expression of TeTX. Ultimately, TeTX inhibits neurotransmitter release by cleaving VAMP2 in synaptic vesicles at nerve endings, thus inhibiting NBNs' function in NBN-TeTX mice noninvasively.

Genotyping

To confirm whether transgenic mice had the desired target recombinant gene, the genotypes of transgenic mice were determined using PCR using DNA extracted from the tails of mice. The tails of mice over three weeks of age were excised by 5 mm and placed in a mixture of proteinase K (protein kinase: Takara Bio Inc., Otsu, Japan) and lysis buffer (100 mM Tris, 5 mM EDTA, 200 mM NaCl, 0.5% Tween-20 pH 8.5), and incubated at 55 °C for more than 12 hours. The DNA was dissolved in 50 μL of TE buffer and used as a template for the PCR reaction. The primer sequences, composition of the reaction solution, and reaction conditions used for the genotyping are depicted in **Figure S1**.

Tamoxifen administration

Tamoxifen was used to stimulate Cre recombinase activity in CreERT2. Tamoxifen was added to a solution of corn oil and 100% ethanol in a 9:1 ratio, and the solution had a tamoxifen concentration of 30 mg/mL. The test tube's outer surface was covered with aluminum foil and incubated for 1 hour at 53 °C with shaking to completely dissolve the tamoxifen. The tubes were then incubated at 37 °C for at least 30 minutes with shaking. The mixture was kept at 37 °C until the mice were administered. For three days, a dose of 180 mg/kg/day was administered intraperitoneally. To determine the dose, body weight was remeasured on each day of administration. Before and after each administration, the needle tip was sterilized with 70% ethanol. To ensure hygiene, a new tamoxifen mixture was prepared every day. To rule out the effect of tamoxifen on the experimental results, all mice used in the experiments (NBN-TeTX group and control group) received tamoxifen injections between the ages of 12 and 14 weeks. Furthermore, all behavioral experiments began three weeks after tamoxifen administration (15 to 17 weeks of age).

BrdU injection

BrdU, the marker of dividing cells, was required to be injected in advance in order to perform immunofluorescence staining of NBNs in the mouse brain at the end of the behavioral experiments. BrdU was diluted in saline to a concentration of 10 mg/mL and injected intraperitoneally at a dose of 0.3 mL/day for three days, which is 3 mg/day.

Introduction of EYFP gene

We transferred the EYFP (Enhanced Yellow Fluorescent Protein) gene into NBN-TeTX mice to visualize NBNs for more accurate statistics on NBN survival. We obtained EYFP-expressing mice from the Jackson laboratory (Srinivas et al., 2001), crossed them with NBN-TeTX mice in our lab to obtain NBN-TeTX-EYFP mice, and then used tissue immunostaining to determine the success of gene introduction. The EYFP gene used in this study also contains the tamoxifen-inducible recombinase CreERT2, which expresses its function after tamoxifen administration, similar to Tg1 in NBN-TeTX mice. Thus, after tamoxifen administration, neural stem cells and precursor cells in mice can express EYFP specifically.

Retrovirus preparation and infection

The previously described Moloney viral vector was used (Nakashiba et al., 2012). All vector concentrations were prepared in TE buffer at 1 g/L (pH 8.0). The retroviral injection was given three days after the tamoxifen administration. After anesthesia, the virus was injected into the right DG using a mineral oil-filled glass micropipette connected to Nanoject II (Drummond). (-2.06 mm AP, 1.25 mm ML, -1.75 mm DV; (-2.7 mm AP, 2.0 mm ML, -1.75 mm DV). At each site, the mice were injected with 0.897 L (69 nL, 13 times) of retrovirus at a rate of 0.8 L/min. The glass micropipette was left at the target site for 3 minutes before being removed.

Fixation, Sectioning, and Immunohistochemistry

Transcardiac perfusion of the mouse brain with PBS (in mM: 137 NaCl, 8.1 Na2HPO4, 2.68 KCl, and 1.47 KH2PO4) and 4% paraformaldehyde (PFA) was performed sequentially. After being fixed at 4°C overnight in 4% PFA and gradient dehydrated with 10%, 20%, and 30% sucrose solutions in 3 days, the brains were embedded in the O.C.T. Compound (Sakura, Tokyo, Japan) and cut into 40 μm coronal or axial slices in a cryostat (Thermo). Immunofluorescence was performed on free-floating sections. TBS (in mM: 137 NaCl, 2.68 KCl, 25 Tris, pH 7.2) was used to wash the slices. Immunofluorescence was performed following standard protocols.

Primary antibodies and dilutions used were as follows: GFP/mcherry: rat monoclonal anti-GFP (dilution 1:2000, Nacalai tesque, Kyoto, Japan) and rabbit polyclonal anti-DsRed (dilution 1:200, Clontech). BrdU: A (dilution 1:200). DCX: doublecortin (C-18) goat polyclonal IgG (dilution 1:200, Santa Cruz Biotechnology). EYFP: rabbit anti-GFP IgG (dilution 1:1000, abcam). NeuN: Ms X Neuronal Nuclei (dilution 1:1000, Millipore). PV: monoclonal anti-parvalbumin antibody produced in mouse (dilution 1:1000), GluR2/3: Rb X Glut Receptor 2&3 (dilution 1:500). c-fos: rabbit polyclonal IgG (dilution 1:200).

Immunofluorescence Image Acquisition and Processing

To quantify the GFP/mCherry co-staining of NBNs at CA3-projecting synapses, images were taken using an oil-immersion lens at 63 magnifications with a confocal microscope (TCS SP2, Leica, Germany). Four slices per mouse were used to count synaptic co-staining over the entire range covering the anterior and posterior dentate gyrus (n = 3 per genotype). In addition to this, all immunolabeled samples were imaged using confocal laser scanning microscopes (FLUOVIEW FV3000, Olympus, Japan) with 20x objectives. In either coronal or axial sections, three slices were randomly selected in the target hippocampal region with typical DG structure, and the average of the bilateral DG target cells was counted and multiplied by the corresponding multiplier to estimate the number of cells in the entire dentate gyrus. The images were captured using a z-stack and a pixel density of 1024 x 1024. Images were processed in the Fluoview Software Module 3 and further processed with Fiji/ImageJ (Schindelin et al., 2012; Schneider et al., 2012), and they were corrected with gradual or minor changes in fluorescence after capture to increase the clarity of each channel during the composite. No changes or adjustments were made selectively to any portion of a specific image.

Selection of behavioral experimental subjects

In all experiments, mice that had all three genes mentioned above were the experimental group, while mice lacking one or both transgenes were used as controls. In addition, for operant-learning experiments performed in fMRI, only male mice were used in both the NBN-TeTX and control groups to exclude differences in BOLD signal and differences in behavioral performance caused by factors such as brain volume differences and anxiety levels. All mice used for behavioral experiments were treated with tamoxifen at 12–14 weeks of age and subjected to experiments between 15–17 weeks. All behavioral experiments were performed during the photoperiod, and the experimenter was blinded to the genotype of the mice used at the time of manipulation. All animal care and treatment procedures conform to the Animal Care and Use Committee of the Graduate School of Frontier Science, University of Tokyo.

Morris Water Maze

To analyze the effect of neuronal functional inhibition on reversal learning, we conducted a 10-day training program and three spatial exploration experiments using 13 NBN-TeTX mice and 11 control mice. The three spatial exploration experiments were located on days 5 (after acquisition learning), 10 (after reversal learning), and 13. A circular pool with a diameter of 120 cm was filled with water and divided equally into four areas (NE, SW, SE, and NW), and a 10-cm-diameter platform was placed 1 cm below the water's surface for the mice to take refuge on. The water temperature was kept between 23°C and 24°C, and a non-toxic white dye was mixed with an opaque color to prevent mice from directly seeing the location of the underwater platform. At the same time, different markings were pasted on the walls around the pool as a cue for the mice to determine the location.

During the 10-day training period (including acquisition learning and reversal learning), the procedure for each training session was as follows: First, mice were placed at random in one of the four areas of the pool as the starting point. The time to reach the platform (latency) was calculated and used as a criterion of spatial memory to evaluate the mice's learning. When the mice reached the platform, they were allowed to rest on it for 15 seconds to memorize the platform's location. The mice were allowed to swim and explore for a maximum of 60 seconds. If they could not reach the platform within the time limit, they were gently guided to the platform with a wooden stick and left on the platform for 15 seconds. Afterward, the mice were wrapped in a dry towel to absorb the water and placed back in their home cage.

Acquisition learning was performed on days 1–5 for five days. Prior to learning, the mice were handled for 5 minutes per day for three consecutive days to familiarize them with the experimenter. The platform was set up in the NE area, and learning was performed six times per day following the previously described procedure. The order was randomized based on ensuring that each starting area was used the same number of times, including one time each for NE near the platform location and two times each for SE and NW away from the platform location, for a total of six times with an interval of 30 seconds between each training session. The first spatial exploration experiment (P1) was conducted immediately after the fifth day of acquisition learning.

Reversal learning was performed after five days of acquisition learning on days 6–10. The platform was moved to the SW region during this period, and learning was performed three times per day. The starting positions were NE, SW, and NW, excluding the region SW where the platform was located; 1 time in each region, for a total of 3 times, with sequential randomization and 30 seconds between each training session. The second spatial exploration trial (P2) was conducted immediately after the inversion learning on day 10.

A total of three spatial exploration trials were conducted after the last day of learning for acquisition learning and inversion learning (Day 5-P1, Day 10-P2) and 72 hours after the end of inversion learning (Day 13-P3). In the spatial exploration test, the platform was removed from the pool, and mice were placed at any point in the pool, ensuring that all mice had the same starting point. P1 and P2 were used to assess the extent of memory during the respective learning processes; after that, a 72-hour forgetting period was set after Day 10 to eliminate the unestablished short-term memory, and P3 was used to confirm what long-term memory had been established for the location of the platform after the entire 10-day learning period. All measurements in this experiment were obtained using the animal experiment analysis software Smart 3.0 (Panlab Harvard Apparatus).

Operant-learning experiment

The operant-learning experiment in this study used an operant-learning apparatus that uses light stimulation to cue mice to lick water and has been used to measure the executive function of the mice accurately. Mice are light-cued while their heads are immobilized in this device, and water is given as a reward when a sensor near their mouths detects a tongue-extending lick in response to the light stimulus **(Fig. 3a)**. This device delivers precise sensory stimulation by immobilizing the mouse's head, and this conditioned reflex is efficiently and successfully established because of the simple relationship between stimulus and response. We used this device to perform Go Task and NoGo Task to investigate the effects of silencing NBNs on executive function.

To fix the mouse's head during the experiments, a series of surgical procedures are required, including removing the hair on the top of the mouse's head after anesthesia, lifting the skin on the top of the skull and cutting it vertically, and making a small circular incision to expose the Bregma. The periosteum is infiltrated with a surface treatment agent for a few seconds before being pivoted to the sides to expose the skull. The Bregma is fitted with a customized resin fixation head plate, with the anterior edge of the head plate avoiding obscuring the mouse's eyes. The mice are returned to their home cage after the surgery and monitored until they are fully awake from anesthesia. The mice were returned to the breeding room and allowed to rest for at least one night before the next step was taken.

Three weeks after tamoxifen injections, mice participating in the experiments were given a three-day handling session to familiarize them with the operators. On the last day of the handling, the mice were restricted to a maximum daily water intake of 2000 μl until the end of the experiment. Following the handling, a three-day reflex-to-light training was conducted. The light cue was constantly on and was briefly turned off when the mice actively licked and were rewarded with water (4μl×2 times). A 10-day Go task was performed after the light-to-lick reflex was established. During this period, the mice were given a light cue of 2 s duration, and if the mice licked voluntarily during this 2 s, they were considered correct and given a water reward. A 15±3-second inter-trial interval (ITI) was set between each trial. Immediately after the Go task, a 10-day NoGo task was performed, during which the mouse was also given a 2-s light cue, was considered correct if it did not lick during this period, and was given water rewards immediately after the light cue.

However, the rules of the operant-learning experiments performed in fMRI are slightly changed **(Fig. 4a)**. First, each trial was set to 20 seconds due to the block design and given a light cue during the initial 2 s (0-2s). Meanwhile, in the NoGo task, the rule was set to be considered correct only when the mouse actively licked within 2 seconds after the light cue went off, to reduce the possibility of false correctness due to mouse inaction (omission) caused by the relatively cold environment and noise during the fMRI scan. That is, the water reward was given only when the subject actually comprehended the rule change and performed the correct licking behavior.

Task-based fMRI analysis

In this study, task-based fMRI imaging was performed at the Graduate School of Frontier Sciences, The University of Tokyo (GSFS). A total of six male NBN-TeTX mice and six male control mice that had completed licking training were included in the study. The scanning was performed with a 14-T high-field small horizontal bore animal scanner (Jastec, Japan). For scanning, a resin head plate, which was previously attached to the skull of the mice, was attached with resin screws to a homemade scanning bed incorporating a manipulative learning experiment, and the mouse Bregma was placed in the center of the acquisition coil, which ensured that its head did not shake greatly during licking. The position of the water tube was adjusted so that the mouse could easily access the water reward. Tripilot images were acquired to ensure correct positioning of the mouse relative to the center of the coil, magnet, etc. tb-fMRI was performed for a total of 180s. The task was designed to give the mouse LED cue at the beginning of the experiment from 0–2 s and wait for 18 s before ending to fully account for the recovery time of the BOLD signal; i.e., every 20 s was one trail, repeated nine times for one scan (180 s), and a

total of 90 sets of fMRI images were obtained (20s × 9 trails). A 10-second window was set before the start of the formal scan to stabilize the fMRI signal. While the Go task and NoGo task were performed, we acquired functional images of the hippocampal region with a Spin Echo-Echo Planar Imaging (SE-EPI) sequence: TR = 2000 ms, TE = 18 ms, FA = 90°, Matrix size = 64 × 64, FOV = 1.72 × 1.72 mm2, slice number = 30, Increasing interleaving, ST = 0.7 mm, slice gap = 0.In addition, T2-weighted whole brain structure images were acquired with the FLASH sequence: TR = 800 ms, TE = 24 ms, FA = 90°, Matrix size = 256 × 256, FOV = 2.27 × 2.27 mm2, slice number=30, Interleaved increasing, slice thickness ST=0.7mm, slice gap=0.

Task-based fMRI data preprocessing was mainly performed using SPM12 (https://www.fil.ion.ucl.ac.uk/spm/software/spm12/) in MATLAB (R2022b) and MRIcroGL (https://www.nitrc.org/projects/mricrogl/). The data preprocessing steps include: (i) image reconstruction, exported in DICOM format and converted to NIfTI format (cm2niix, MRIcroGL), which also included slicing time correction (slicing time, SPM12); (ii) manual rotation and flipping of the images so that the origin of the coordinates occupied the midpoint of the forebrain comma to approximately match the standard reference space (SPM12). (iii) nominal voxel size magnification by a factor of 10 to facilitate image processing (SPM12); (iv) discarding the first 10s EPI images at the beginning of each individual scan; (v) correcting the motion of the EPI images (realignment to mean, SPM12); (vi) using the Allen Mouse Brain Common Coordinate Framework (Wang et al., 2020) (P56_Atlas_downsample2.nii.) structural images as a standard template to normalize the individual anatomical images (struc. image normalization, SPM12); (vii) using the standardized individual anatomical images as a template to align the individual functional images with images coregister (SPM12); (viii) segmentation of the normalized individual anatomical images using the composition template to better distinguish between white matter, gray matter, cerebrospinal fluid, bone, and air (segment, SPM12); (ix) segmentation of the normalized individual anatomical images using the completed Normalization and Segment's structural images were used as templates to normalize individual EPI images with (func. images normalization, SPM12); (x) EPI images were smoothed with a FWHM maximum of 0.4 mm (smooth, SPM12); (xi) In 1st-level Analysis by multiple regression analysis to remove six head motion parameters as well as the average signal of white matter and ventricles (SPM12). The images were drawn at $p < 0.05$ FDR-corrected.

Resting-state fMRI analysis

In this study, rs-fMRI imaging was performed at the Okinawa Institute of Science and Technology Graduate University (OIST). 14 NBN-TeTX mice and 14 control mice have participated. Each mouse was anesthetized with isoflurane (3% for initial induction and 1.5% during MRI scanning) and was placed in the prone position on a custom-built MRI bed with a bite bar and a gas mask. Core body temperature was monitored throughout the scan using an MRI-compatible temperature probe (Model 1025, SA Instruments, Stony Brook, NY, USA) inserted into the rectum and regulated at 37.0 ± 1.0 °C using a water-circulating pad. MRI data were acquired with an 11.7-T small horizontal bore animal scanner (BioSpec 117/11, Bruker, Ettlingen, Germany), a mouse head-adapted cryocoil, and ParaVision 6.0.1 software. Tripilot images were acquired to ensure the correct positioning of mice concerning the coil and the magnet isocenter. Resting-state fMRI was conducted for 6 min, with blood oxygenation level-dependent (BOLD) spin-echo echo-planar images (EPI) acquired using repetition time = 1800 ms, echo time = 18 ms, flip angle = 90°, matrix size = 96 × 96, field of view = 20 × 20 mm2, slice number = 22, slice thickness ST = 0.5 mm, slice gap = 0, and bandwidth BW = 500 kHz, 200 volumes. T2-weighted anatomical images were also acquired using repetition time = 3374

ms, echo time = 30 ms, flip angle = 90°, matrix size = 256 × 256, field of view = 20 × 20mm2, slice number = 34, slice thickness ST = 0.5 mm, slice gap = 0, and number of averages = 2. Resting-state fMRI data were processed using SPM12 (https://www.fil.ion.ucl.ac.uk/spm/) and CONN (Whitfield-Gabrieli and Nieto-Castanon, 2012). Data preprocessing steps included: (i) image was reconstructed and exported in DICOM format and converted to NIfTI format (dcm2niix, MRIcroGL), which also includes slice timing correction; (ii) image was manually rotated and translated such that the origin of the coordinates occupied the midpoint of the anterior commissure to roughly match the standard reference space (SPM12); (iii) the nominal voxel size was enlarged 10 times to facilitate image processing (SPM12); (iv) the first 10 volumes of EPI images were discarded; (v) the motion of EPI images was corrected (SPM12); (vi) the mean of EPI images were used to create a study specific template (SPM12); (vii) the T2 anatomical images were used to create a study specific template (SPM12); (viii) the EPI template is linearly and nonlinearly coregistered to the T2 template and finally to the Allen Mouse Brain Common Coordinate Framework atlas (SPM12); (ix) the EPI images were normalized to atlas template and resampled into 100 isotropic voxels (SPM12); (x) the EPI images were smoothed with a full-width at half-maximum at 0.4 mm (SPM12); (xi) the 6 head motion parameters, along with averaged signals from white matter, cerebrospinal fluid and ventricles were removed by multiple regressing analysis (CONN); (xii) the EPI images were temporally filtered between 0.01 and 0.1 Hz (CONN); and finally (xiii) the correlation coefficient between each ROI were computed and plot the results (CONN). 3D Slicer (Fedorov et al., 2012) was used for the segmentation and production of the regions of interest (ROI).

Statistical analysis

Statistics for immunofluorescence staining were performed using student's t-test or two-sample t-test, as needed. Behavioral experiments statistics were performed using student's t-test or two-way repeated-measures ANOVA with post hoc Bonferroni test, as needed. The main analysis was performed using GraphPad Prism 9.4.0 (673) for Windows. fMRI correlation analysis was performed using the software's built-in algorithm. $P<0.05$ as a criterion of significance, and all values are reported as mean±SEM.

Data and code availability

Microscopy data reported in this paper will be shared by the lead contact upon request. Any additional information required to reanalyze the data reported in this paper is available from the lead contact upon request.

Acknowledgments

We are grateful to Prof. Ryoichiro Kageyama and Prof. Itaru Imayoshi for their generous support of the mouse models needed for this experiment. We thank Dr. Toshiaki Nakashiba for the gift of Moloney virus. We also thank students Qiong Ding and Shuto Mine for their help in data collection. The first author would like to extend the deepest gratitude to Dr. Zekun Cai, whose unwavering support and inspiration shone like a star in the darkest of nights, illuminating a path forward during the most bewildering moments. This research was supported by the Graduate School of Frontier Sciences, The University of Tokyo, through the Challenging New Area Doctoral Research Grant (Project No. A22032). Some of the diagrams in the article were created with BioRender.com.

Author Contributions

Conceptualization, H.L., R.T., H.A., K.Z.T., T.J.M. and T.H.; Methodology, H.L., R.T., D.H.,

H.A., J. Koga., S.A., K.S. K.Z.T., T.J.M. and T.H.; Data Collection, H.L., S.Y., Q.D., J. Kaneko, T.Y., K.H. and T.H.; Data Analysis, H.L., J. Koga, K.S., A.S. and T.H.; Funding, T.H.; Supervision, T.J.M. and T.H.; Writing, H.L., T.J.M. and T.H.

Reference

1. Aimone, J.B., Wiles, J., and Gage, F.H. (2006). Potential role for adult neurogenesis in the encoding of time in new memories. Nat Neurosci *9*, 723-727.
2. Aimone, J.B., Wiles, J., and Gage, F.H. (2009). Computational influence of adult neurogenesis on memory encoding. Neuron *61*, 187-202.
3. Amaral, D.G., Scharfman, H.E., and Lavenex, P. (2007). The dentate gyrus: fundamental neuroanatomical organization (dentate gyrus for dummies). Prog Brain Res *163*, 3-22.
4. Ambrogini, P., Orsini, L., Mancini, C., Ferri, P., Ciaroni, S., and Cuppini, R. (2004). Learning may reduce neurogenesis in adult rat dentate gyrus. Neurosci Lett *359*, 13-16.
5. Anacker, C., and Hen, R. (2017). Adult hippocampal neurogenesis and cognitive flexibility - linking memory and mood. Nat Rev Neurosci *18*, 335-346.
6. Anderson, M.C., and Hanslmayr, S. (2014). Neural mechanisms of motivated forgetting. Trends Cogn Sci *18*, 279-292.
7. Burghardt, N.S., Park, E.H., Hen, R., and Fenton, A.A. (2012). Adult-born hippocampal neurons promote cognitive flexibility in mice. Hippocampus *22*, 1795-1808.
8. Chen, Q.N., Ding, X.L., Guo, X.X., Zhou, G., and Guan, J.S. (2022). Suv39h1 regulates memory stability by inhibiting the expression of Shank1 in hippocampal newborn neurons. Eur J Neurosci *55*, 1424-1441.
9. Clelland, C.D., Choi, M., Romberg, C., Clemenson, G.D., Fragniere, A., Tyers, P., Jessberger, S., Saksida, L.M., Barker, R.A., Gage, F.H.*, et al.* (2009). A Functional Role for Adult Hippocampal Neurogenesis in Spatial Pattern Separation. Science *325*, 210-213.
10. Collins, A., and Koechlin, E. (2012). Reasoning, Learning, and Creativity: Frontal Lobe Function and Human Decision-Making. Plos Biol *10*.
11. Creer, D.J., Romberg, C., Saksida, L.M., van Praag, H., and Bussey, T.J. (2010). Running enhances spatial pattern separation in mice. P Natl Acad Sci USA *107*, 2367-2372.
12. Denny, C.A., Burghardt, N.S., Schachter, D.M., Hen, R., and Drew, M.R. (2012). 4-to 6-week-old adult-born hippocampal neurons influence novelty-evoked exploration and contextual fear conditioning. Hippocampus *22*, 1188-1201.
13. Diamond, A. (2013). Executive functions. Annu Rev Psychol *64*, 135-168.
14. Dieni, C.V., Chancey, J.H., and Overstreet-Wadiche, L.S. (2013). Dynamic functions of GABA signaling during granule cell maturation. Front Neural Circuit *6*.
15. Dinh, T.N.A., Jung, W.B., Shim, H.J., and Kim, S.G. (2021). Characteristics of fMRI responses to visual stimulation in anesthetized vs. awake mice. Neuroimage *226*, 117542.
16. Drew, L.J., Kheirbek, M.A., Luna, V.M., Denny, C.A., Cloidt, M.A., Wu, M.V., Jain, S., Scharfman, H.E., and Hen, R. (2016). Activation of Local Inhibitory Circuits in the Dentate Gyrus by Adult-Born Neurons. Hippocampus *26*, 763-778.
17. Dupret, D., Fabre, A., Dobrossy, M.D., Panatier, A., Rodriguez, J.J., Lamarque, S., Lemaire, V., Oliet, S.H., Piazza, P.V., and Abrous, D.N. (2007a). Spatial learning depends on both the addition and removal of new hippocampal neurons. Plos Biol *5*, e214.
18. Dupret, D., Fabre, A., Dobrossy, M.D., Panatier, A., Rodriguez, J.J., Lamarque, S., Lemaire, V., Oliet, S.H.R., Piazza, P.V., and Abrous, D.N. (2007b). Spatial learning depends on both the addition and removal of new hippocampal neurons. Plos Biol *5*, 1683-1694.
19. Dupret, D., Revest, J.M., Koehl, M., Ichas, F., De Giorgi, F., Costet, P., Abrous, D.N., and Piazza, P.V. (2008). Spatial Relational Memory Requires Hippocampal Adult Neurogenesis. Plos One *3*.
20. Epp, J.R., Silva Mera, R., Kohler, S., Josselyn, S.A., and Frankland, P.W. (2016). Neurogenesis-mediated forgetting minimizes proactive interference. Nat Commun *7*, 10838.
21. Fanselow, M.S., and Dong, H.W. (2010). Are the Dorsal and Ventral Hippocampus Functionally Distinct Structures? Neuron *65*, 7-19.
22. Fedorov, A., Beichel, R., Kalpathy-Cramer, J., Finet, J., Fillion-Robin, J.C., Pujol, S., Bauer, C., Jennings, D., Fennessy, F., Sonka, M.*, et al.* (2012). 3D Slicer as an image computing platform for the Quantitative Imaging Network. Magn Reson Imaging *30*, 1323-1341.
23. Ferecsko, A.S., Jiruska, P., Foss, L., Powell, A.D., Chang, W.C., Sik, A., and Jefferys, J.G. (2015). Structural and functional substrates of tetanus toxin in an animal model of temporal lobe epilepsy. Brain Struct Funct *220*,

1013-1029.
24. Fredes, F., Silva, M.A., Koppensteiner, P., Kobayashi, K., Joesch, M., and Shigemoto, R. (2021). Ventro-dorsal Hippocampal Pathway Gates Novelty-Induced Contextual Memory Formation. Curr Biol *31*, 25-+.
25. Garthe, A., Behr, J., and Kempermann, G. (2009). Adult-Generated Hippocampal Neurons Allow the Flexible Use of Spatially Precise Learning Strategies. Plos One *4*.
26. Ge, S., Goh, E.L., Sailor, K.A., Kitabatake, Y., Ming, G.L., and Song, H. (2006). GABA regulates synaptic integration of newly generated neurons in the adult brain. Nature *439*, 589-593.
27. Ge, S., Yang, C.H., Hsu, K.S., Ming, G.L., and Song, H. (2007). A critical period for enhanced synaptic plasticity in newly generated neurons of the adult brain. Neuron *54*, 559-566.
28. Hainmueller, T., and Bartos, M. (2020). Dentate gyrus circuits for encoding, retrieval and discrimination of episodic memories. Nat Rev Neurosci *21*, 153-168.
29. Han, Z., Chen, W., Chen, X., Zhang, K., Tong, C., Zhang, X., Li, C.T., and Liang, Z. (2019). Awake and behaving mouse fMRI during Go/No-Go task. Neuroimage *188*, 733-742.
30. Hara, T., Nakamura, K., Matsui, M., Yamamoto, A., Nakahara, Y., Suzuki-Migishima, R., Yokoyama, M., Mishima, K., Saito, I., Okano, H.*, et al.* (2006). Suppression of basal autophagy in neural cells causes neurodegenerative disease in mice. Nature *441*, 885-889.
31. Heigele, S., Sultan, S., Toni, N., and Bischofberger, J. (2016). Bidirectional GABAergic control of action potential firing in newborn hippocampal granule cells. Nat Neurosci *19*, 263-270.
32. Hsu, T.T., Lee, C.T., Tai, M.H., and Lien, C.C. (2016). Differential Recruitment of Dentate Gyrus Interneuron Types by Commissural Versus Perforant Pathways. Cereb Cortex *26*, 2715-2727.
33. Huckleberry, K.A., Shue, F., Copeland, T., Chitwood, R.A., Yin, W., and Drew, M.R. (2018). Dorsal and ventral hippocampal adult-born neurons contribute to context fear memory. Neuropsychopharmacology *43*, 2487-2496.
34. Ide, Y., Fujiyama, F., Okamoto-Furuta, K., Tamamaki, N., Kaneko, T., and Hisatsune, T. (2008). Rapid integration of young newborn dentate gyrus granule cells in the adult hippocampal circuitry. European Journal of Neuroscience *28*, 2381-2392.
35. Ikrar, T., Guo, N., He, K., Besnard, A., Levinson, S., Hill, A., Lee, H.K., Hen, R., Xu, X., and Sahay, A. (2013). Adult neurogenesis modifies excitability of the dentate gyrus. Front Neural Circuits *7*, 204.
36. Imayoshi, I., Ohtsuka, T., Metzger, D., Chambon, P., and Kageyama, R. (2006). Temporal regulation of Cre recombinase activity in neural stem cells. Genesis *44*, 233-238.
37. Imayoshi, I., Sakamoto, M., Ohtsuka, T., Takao, K., Miyakawa, T., Yamaguchi, M., Mori, K., Ikeda, T., Itohara, S., and Kageyama, R. (2008). Roles of continuous neurogenesis in the structural and functional integrity of the adult forebrain. Nat Neurosci *11*, 1153-1161.
38. Kempermann, G. (2015). Activity Dependency and Aging in the Regulation of Adult Neurogenesis. Cold Spring Harb Perspect Biol *7*.
39. Kempermann, G., Kuhn, H.G., and Gage, F.H. (1997). More hippocampal neurons in adult mice living in an enriched environment. Nature *386*, 493-495.
40. Komatsu, M., Waguri, S., Chiba, T., Murata, S., Iwata, J., Tanida, I., Ueno, T., Koike, M., Uchiyama, Y., Kominami, E.*, et al.* (2006). Loss of autophagy in the central nervous system causes neurodegeneration in mice. Nature *441*, 880-884.
41. Lacefield, C.O., Itskov, V., Reardon, T., Hen, R., and Gordon, J.A. (2012). Effects of adult-generated granule cells on coordinated network activity in the dentate gyrus. Hippocampus *22*, 106-116.
42. Leutgeb, J.K., Leutgeb, S., Moser, M.B., and Moser, E.I. (2007). Pattern separation in the dentate gyrus and CA3 of the hippocampus. Science *315*, 961-966.
43. Luftman, K., Hasan, N., Day, P., Hardee, D., and Hu, C. (2009). Silencing of VAMP3 inhibits cell migration and integrin-mediated adhesion. Biochem Biophys Res Commun *380*, 65-70.
44. Maletic-Savatic, M., Malinow, R., and Svoboda, K. (1999). Rapid dendritic morphogenesis in CA1 hippocampal dendrites induced by synaptic activity. Science *283*, 1923-1927.
45. Matsuzaki, M., Honkura, N., Ellis-Davies, G.C., and Kasai, H. (2004). Structural basis of long-term potentiation in single dendritic spines. Nature *429*, 761-766.
46. McAvoy, K., Besnard, A., and Sahay, A. (2015). Adult hippocampal neurogenesis and pattern separation in DG: a role for feedback inhibition in modulating sparseness to govern population-based coding. Front Syst Neurosci *9*, 120.
47. McHugh, S.B., Lopes-Dos-Santos, V., Gava, G.P., Hartwich, K., Tam, S.K.E., Bannerman, D.M., and Dupret, D.

(2022). Adult-born dentate granule cells promote hippocampal population sparsity. Nat Neurosci *25*, 1481-1491.
48. McHugh, T.J., Jones, M.W., Quinn, J.J., Balthasar, N., Coppari, R., Elmquist, J.K., Lowell, B.B., Fanselow, M.S., Wilson, M.A., and Tonegawa, S. (2007). Dentate gyrus NMDA receptors mediate rapid pattern separation in the hippocampal network. Science *317*, 94-99.
49. Ming, G.L., and Song, H.J. (2011). Adult Neurogenesis in the Mammalian Brain: Significant Answers and Significant Questions. Neuron *70*, 687-702.
50. Miyake, A., Friedman, N.P., Emerson, M.J., Witzki, A.H., Howerter, A., and Wager, T.D. (2000). The unity and diversity of executive functions and their contributions to complex "Frontal Lobe" tasks: a latent variable analysis. Cogn Psychol *41*, 49-100.
51. Monk, C.S., Zhuang, J.C., Curtis, W.J., Ofenloch, I.T., Tottenham, N., Nelson, C.A., and Hu, X.P. (2002). Human hippocampal activation in the delayed matching- and nonmatching-to-sample memory tasks: An event-related functional MRI approach. Behav Neurosci *116*, 716-721.
52. Nakashiba, T., Cushman, J.D., Pelkey, K.A., Renaudineau, S., Buhl, D.L., McHugh, T.J., Barrera, V.R., Chittajallu, R., Iwamoto, K.S., McBain, C.J.*, et al.* (2012). Young Dentate Granule Cells Mediate Pattern Separation, whereas Old Granule Cells Facilitate Pattern Completion. Cell *149*, 188-201.
53. Nakashiba, T., Young, J.Z., McHugh, T.J., Buhl, D.L., and Tonegawa, S. (2008). Transgenic inhibition of synaptic transmission reveals role of CA3 output in hippocampal learning. Science *319*, 1260-1264.
54. O'Leary, O.F., and Cryan, J.F. (2014). A ventral view on antidepressant action: roles for adult hippocampal neurogenesis along the dorsoventral axis. Trends Pharmacol Sci *35*, 675-687.
55. Pilz, G.A., Bottes, S., Betizeau, M., Jorg, D.J., Carta, S., Simons, B.D., Helmchen, F., and Jessberger, S. (2018). Live imaging of neurogenesis in the adult mouse hippocampus. Science *359*, 658-662.
56. Poppenk, J., Evensmoen, H.R., Moscovitch, M., and Nadel, L. (2013). Long-axis specialization of the human hippocampus. Trends Cogn Sci *17*, 230-240.
57. Puri, C., Renna, M., Bento, C.F., Moreau, K., and Rubinsztein, D.C. (2013). Diverse autophagosome membrane sources coalesce in recycling endosomes. Cell *154*, 1285-1299.
58. Ryan, T.J., and Frankland, P.W. (2022). Forgetting as a form of adaptive engram cell plasticity. Nat Rev Neurosci *23*, 173-186.
59. Sagar, S.M., Sharp, F.R., and Curran, T. (1988). Expression of c-fos protein in brain: metabolic mapping at the cellular level. Science *240*, 1328-1331.
60. Sakurai, K., Shintani, T., Jomura, N., Matsuda, T., Sumiyoshi, A., and Hisatsune, T. (2020). Hyper BOLD Activation in Dorsal Raphe Nucleus of APP/PS1 Alzheimer's Disease Mouse during Reward-Oriented Drinking Test under Thirsty Conditions. Sci Rep *10*, 3915.
61. Scharfman, H.E. (1995). Electrophysiological Evidence That Dentate Hilar Mossy Cells Are Excitatory and Innervate Both Granule Cells and Interneurons. J Neurophysiol *74*, 179-194.
62. Scharfman, H.E. (2016). The enigmatic mossy cell of the dentate gyrus. Nat Rev Neurosci *17*, 562-575.
63. Scharfman, H.E., and Myers, C.E. (2012). Hilar mossy cells of the dentate gyrus: a historical perspective. Front Neural Circuits *6*, 106.
64. Schindelin, J., Arganda-Carreras, I., Frise, E., Kaynig, V., Longair, M., Pietzsch, T., Preibisch, S., Rueden, C., Saalfeld, S., Schmid, B.*, et al.* (2012). Fiji: an open-source platform for biological-image analysis. Nat Methods *9*, 676-682.
65. Schneider, C.A., Rasband, W.S., and Eliceiri, K.W. (2012). NIH Image to ImageJ: 25 years of image analysis. Nat Methods *9*, 671-675.
66. Small, D.M., Zatorre, R.J., Dagher, A., Evans, A.C., and Jones-Gotman, M. (2001). Changes in brain activity related to eating chocolate: from pleasure to aversion. Brain *124*, 1720-1733.
67. Spalding, K.L., Bergmann, O., Alkass, K., Bernard, S., Salehpour, M., Huttner, H.B., Bostrom, E., Westerlund, I., Vial, C., Buchholz, B.A.*, et al.* (2013). Dynamics of Hippocampal Neurogenesis in Adult Humans. Cell *153*, 1219-1227.
68. Squire, L.R. (1992). Memory and the Hippocampus - a Synthesis from Findings with Rats, Monkeys, and Humans. Psychol Rev *99*, 195-231.
69. Srinivas, S., Watanabe, T., Lin, C.S., William, C.M., Tanabe, Y., Jessell, T.M., and Costantini, F. (2001). Cre reporter strains produced by targeted insertion of EYFP and ECFP into the ROSA26 locus. BMC Dev Biol *1*, 4.
70. Strange, B.A., Witter, M.P., Lein, E.S., and Moser, E.I. (2014a). Functional organization of the hippocampal longitudinal axis. Nat Rev Neurosci *15*, 655-669.

71. Strange, B.A., Witter, M.P., Lein, E.S., and Moser, E.I. (2014b). Functional organization of the hippocampal longitudinal axis. Nat Rev Neurosci *15*, 655-669.
72. Sun, B., Halabisky, B., Zhou, Y., Palop, J.J., Yu, G., Mucke, L., and Gan, L. (2009). Imbalance between GABAergic and Glutamatergic Transmission Impairs Adult Neurogenesis in an Animal Model of Alzheimer's Disease. Cell Stem Cell *5*, 624-633.
73. Swan, A.A., Clutton, J.E., Chary, P.K., Cook, S.G., Liu, G.G., and Drew, M.R. (2014). Characterization of the Role of Adult Neurogenesis in Touch-Screen Discrimination Learning. Hippocampus *24*, 1581-1591.
74. Tashiro, A., Makino, H., and Gage, F.H. (2007). Experience-specific functional modification of the dentate gyrus through adult neurogenesis: a critical period during an immature stage. J Neurosci *27*, 3252-3259.
75. Taupin, P., and Gage, F.H. (2002). Adult neurogenesis and neural stem cells of the central nervous system in mammals. J Neurosci Res *69*, 745-749.
76. Toda, T., Parylak, S.L., Linker, S.B., and Gage, F.H. (2019). The role of adult hippocampal neurogenesis in brain health and disease. Mol Psychiatry *24*, 67-87.
77. Toni, N., Laplagne, D.A., Zhao, C., Lombardi, G., Ribak, C.E., Gage, F.H., and Schinder, A.F. (2008). Neurons born in the adult dentate gyrus form functional synapses with target cells. Nat Neurosci *11*, 901-907.
78. Toni, N., and Schinder, A.F. (2016). Maturation and Functional Integration of New Granule Cells into the Adult Hippocampus. Csh Perspect Biol *8*.
79. Tozuka, Y., Fukuda, S., Namba, T., Seki, T., and Hisatsune, T. (2005). GABAergic excitation promotes neuronal differentiation in adult hippocampal progenitor cells. Neuron *47*, 803-815.
80. Voss, J.L., Bridge, D.J., Cohen, N.J., and Walker, J.A. (2017). A Closer Look at the Hippocampus and Memory. Trends in Cognitive Sciences *21*, 577-588.
81. Wang, Q., Ding, S.L., Li, Y., Royall, J., Feng, D., Lesnar, P., Graddis, N., Naeemi, M., Facer, B., Ho, A.*, et al.* (2020). The Allen Mouse Brain Common Coordinate Framework: A 3D Reference Atlas. Cell *181*, 936-953 e920.
82. Whitfield-Gabrieli, S., and Nieto-Castanon, A. (2012). Conn: a functional connectivity toolbox for correlated and anticorrelated brain networks. Brain Connect *2*, 125-141.
83. Wu, X., Fleming, A., Ricketts, T., Pavel, M., Virgin, H., Menzies, F.M., and Rubinsztein, D.C. (2016). Autophagy regulates Notch degradation and modulates stem cell development and neurogenesis. Nat Commun *7*, 10533.
84. Yamamoto, M., Wada, N., Kitabatake, Y., Watanabe, D., Anzai, M., Yokoyama, M., Teranishi, Y., and Nakanishi, S. (2003). Reversible suppression of glutamatergic neurotransmission of cerebellar granule cells in vivo by genetically manipulated expression of tetanus neurotoxin light chain. J Neurosci *23*, 6759-6767.
85. Yau, S.Y., Li, A., and So, K.F. (2015). Involvement of Adult Hippocampal Neurogenesis in Learning and Forgetting. Neural Plast *2015*.
86. Zhao, C., Deng, W., and Gage, F.H. (2008). Mechanisms and functional implications of adult neurogenesis. Cell *132*, 645-660.

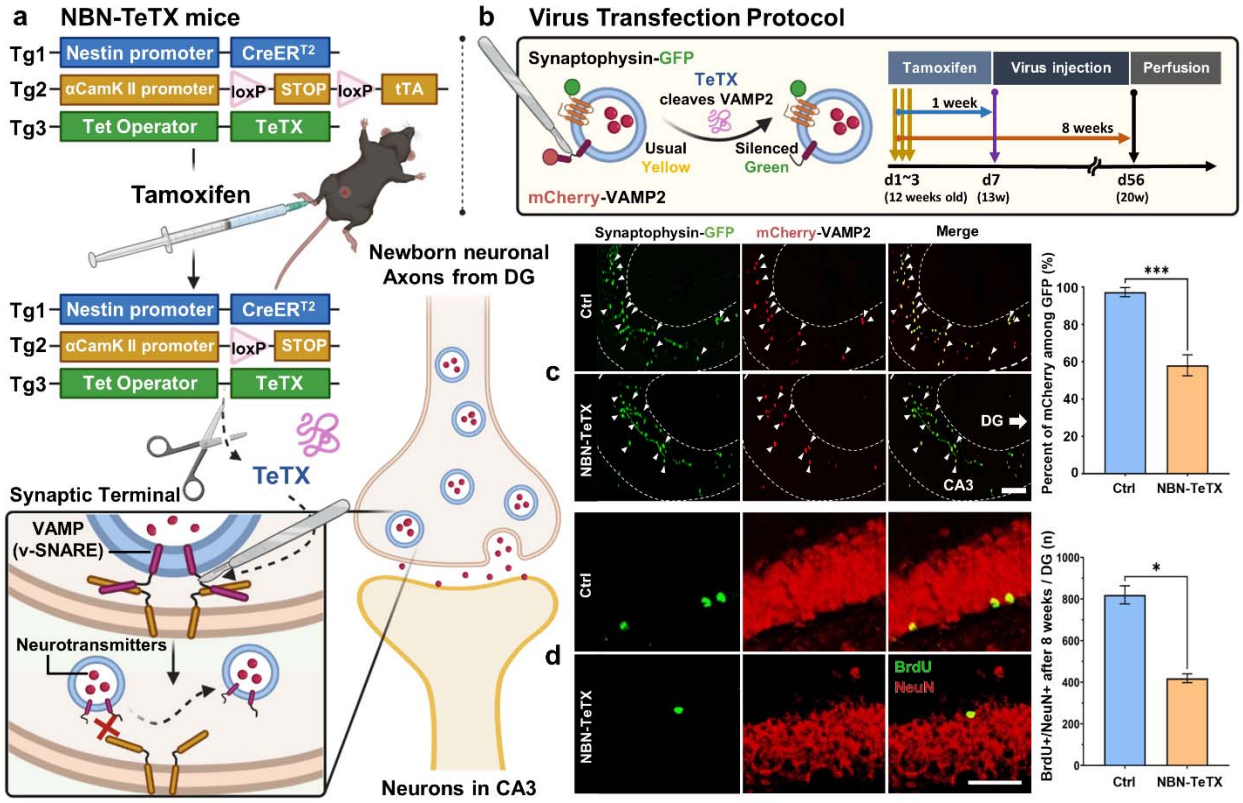

Figure 1. Genetic composition of NBN-TeTX (Newborn Neuron – Tetanus Toxin expressing) mice.

a. Shows the genetic composition of NBN-TeTX mice and the mechanism of silencing newborn neurons. In this mouse model with three recombinant genes, CreERT2 is expressed in Nestin-positive neural stem/progenitor cells and stays in the cytoplasm, then translocated into the nucleus upon tamoxifen injection and removed the STOP codon of Tg2. When these cells differentiate into neurons, the αCamKII promoter is activated, and tTA is expressed. tTA binds to the Tet Operator of Tg3, which expresses downstream TeTX. Then, TeTX expressed at synaptic terminals inhibits neurotransmitter release by cleaving VAMP2 of synaptic vesicles at synaptic terminals and thus specifically silencing newborn neurons.

b. Two fluorescent markers of synaptic vesicles, synaptophysin-GFP, and VAMP2-mCherry, were co-expressed at synaptic endings by viral transfection. Retroviral injections were performed a few days after tamoxifen administration, and perfusion and staining were performed 8 weeks later.

c. Approximately 40% of synaptic terminals in Tg mice contained shed mCherry, whereas there was almost no shed mCherry in the control group. Synaptophysin-GFP+ and VAMP2-mCherry- synapses are shown at arrowheads. (Tg: Average=58.003±3.366, Ctrl: Average=97.265±1.382, ***$p < 0.001$; student's t-test, scale bar: 100 µm.)

d. The number of surviving newborn neurons was significantly decreased in NBN-TeTX mice after 8 weeks of tamoxifen injection. (NBN-TeTX: n=6, Ctrl: n=6, *$p<0.05$, student's t-test, scale bar=50µm)

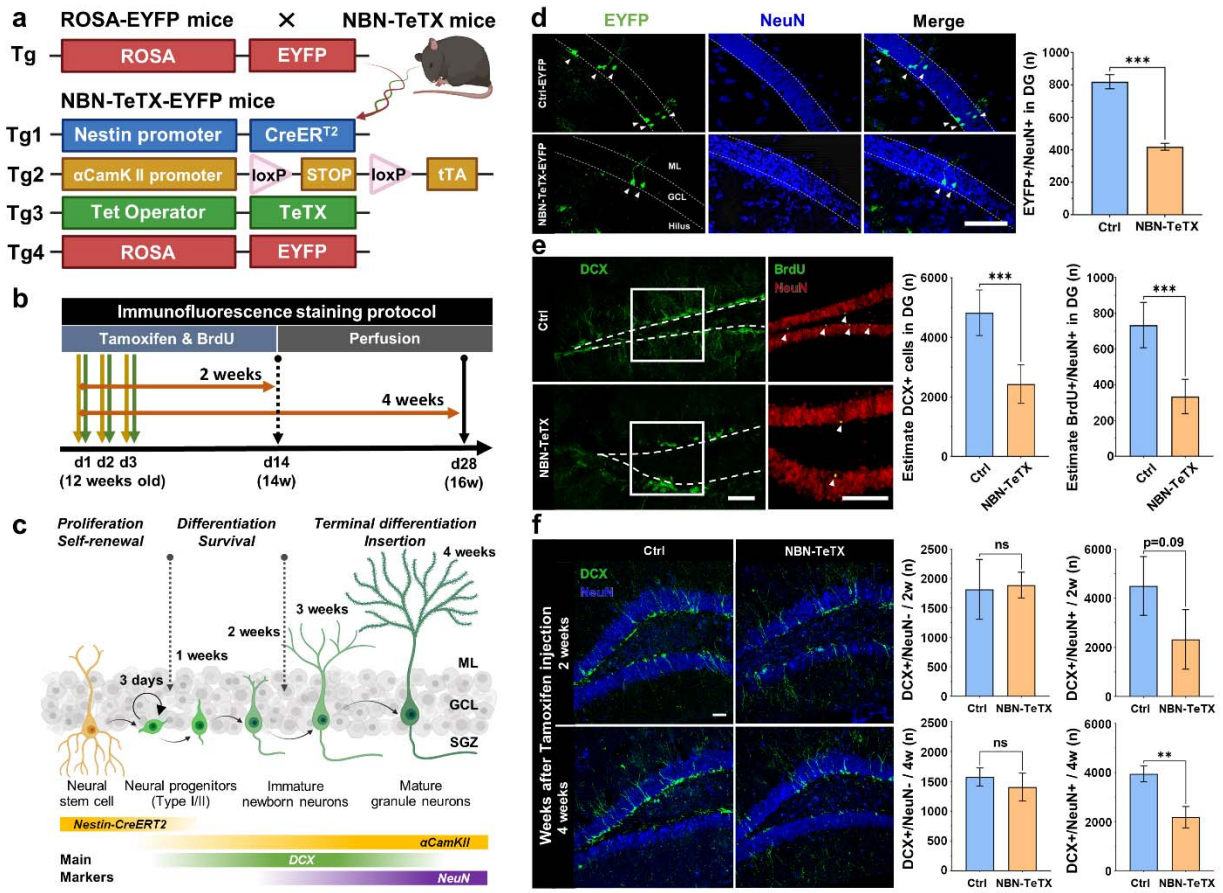

Figure 2. Reduction of 2-4-week-old surviving newborn neurons in NBN-TeTX mice

a. To directly observe the number of surviving newborn neurons, NBN-TeTX mice were crossed with ROSA-EYFP mice, and NBN-TeTX-EYFP mice containing four transgenes were obtained. Thus, EYFP was expressed in newborn neurons simultaneously with tamoxifen injection.

b. The activation schedule for the NBN-TeTX mouse model. The immunofluorescence staining and behavioral experiments in this study began by administering tamoxifen (including BrdU injection) for three consecutive days to mice at 12 to 14 weeks of age. To determine when tamoxifen took effect, immunofluorescence staining was performed at 2 and 4 weeks after injection. See Fig.2f for details.

c. A time-scale schematic of the adult hippocampal neurogenesis that occurs in the subgranular zone of the dentate gyrus. Using the difference in the time windows of DCX and NeuN expression, we were able to approximate the time period during which tamoxifen caused a decrease in the number of newborn neurons.

d. EYFP+ staining performed at the fourth week post-injection showed that the hippocampal dentate gyrus EYFP+ cells of NBN-TeTX mice were significantly reduced by approximately 50% compared to controls. (NBN-TeTX: n=6, Ctrl: n=5, ***p<0.001, student's t-test, scale bar=50μm.)

e. Simultaneous DCX+ and BrdU+/NeuN+ immunofluorescence staining results were consistent with the EYFP+ results. the number of surviving newborn neurons was significantly decreased in NBN-TeTX mice. (DCX: NBN-TeTX: n=6, Ctrl: n=6, ***p<0.001, student's t-test, scale bar=100μm; BrdU/NeuN: NBN-TeTX: n=6, Ctrl: n=6, ***p<0.001, student's t-test, scale bar=80

µm.)

f. Immunofluorescence staining performed 2 weeks (left) after tamoxifen injection revealed no significant differences between the Ctrl and NBN-TeTX groups for progenitor cells represented by DCX+/NeuN- and immature neurons represented by DCX+/NeuN+ (NBN-TeTX: n=3, Ctrl: n=3). At week 4 post-injection, however, immunofluorescence revealed a significant decrease in immature newborn neurons (DCX+/NeuN+) in the NBN-TeTX group compared to the control group (NBN-TeTX: n=3, Ctrl: n=3, **$p<0.01$, student's t-test, scale bar=50µm;). While their progenitor cell (DCX+/NeuN-) counts were also reduced, they were not statistically different.

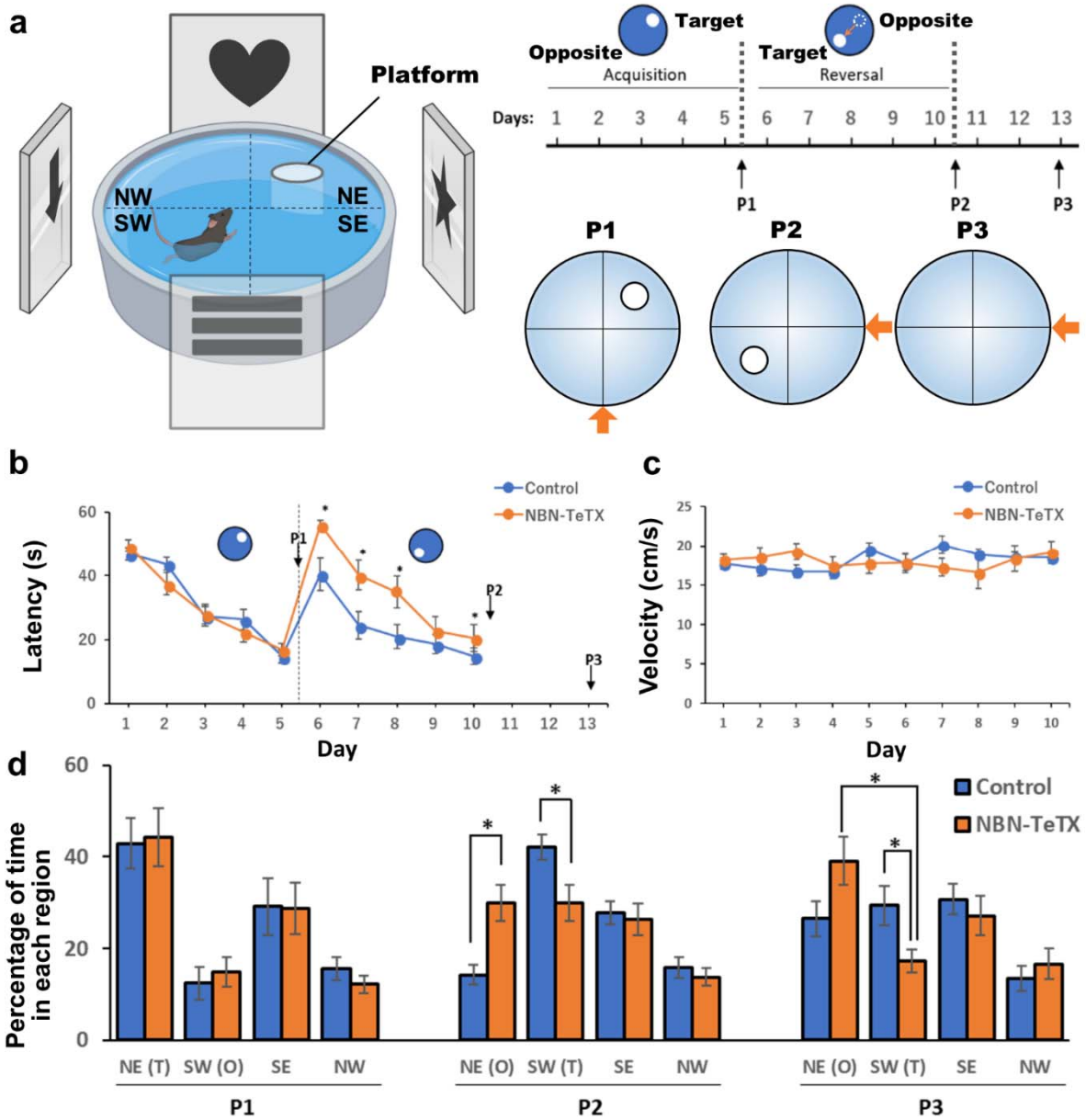

Figure 3. Silencing newborn neurons impedes reversal learning in Morris water maze.

a. Morris water maze test experimental scheme for measuring reversal learning. In the 5-day acquisition learning (D1-5), the platform was located in the NE zone, while in the subsequent 5-day reversal learning (D5-10), the platform was moved to the SW regions. Probe test P1 and P2 were conducted immediately after the last day of acquisition and reversal learning, respectively. P3 was scheduled on day 13 to detect final memory regarding the platform location. The starting position of the mice swimming during the three probe tests is shown by the orange arrow.
b. Escape Latency (s) of the 10-day training session showed that both groups showed similar learning trends in initial acquisition learning (D1-5), but showed a major effect from genotype during reversal learning (D6-10). (Reversal learning: NBN-TeTX: n=13, Ctrl: n=11, genotype: $F(1, 22)=7.8367$, $p=0.0104$, $*p<0.05$, two-way repeated measures ANOVA with post hoc Bonferroni test).
c. Moving speed (cm/s) throughout the 10-day training session between groups.

d. Percentage of exploring time spent in each zone by the two groups in the three probe tests. During P1, no significant difference was observed, but during P2, significant differences were observed between the two groups in the time spent in the NE(O) and SW(T) zones (zone NE: $p=0.0045$, zone SW: $p=0.0285$; $*p<0.05$; student's t-test). In contrast, a significant difference in exploration time during P3 between two groups was observed only in the SW(T) zone (zone SW: $p=0.0232$). Besides, Tg group also showed a significant difference in exploration time between the NE(O) and SW(T). (Between zone NE and SW: NBN-TeTX: $p=0.0015$; $*p<0.05$; Ctrl: $p=0.6394$, student's t-test).

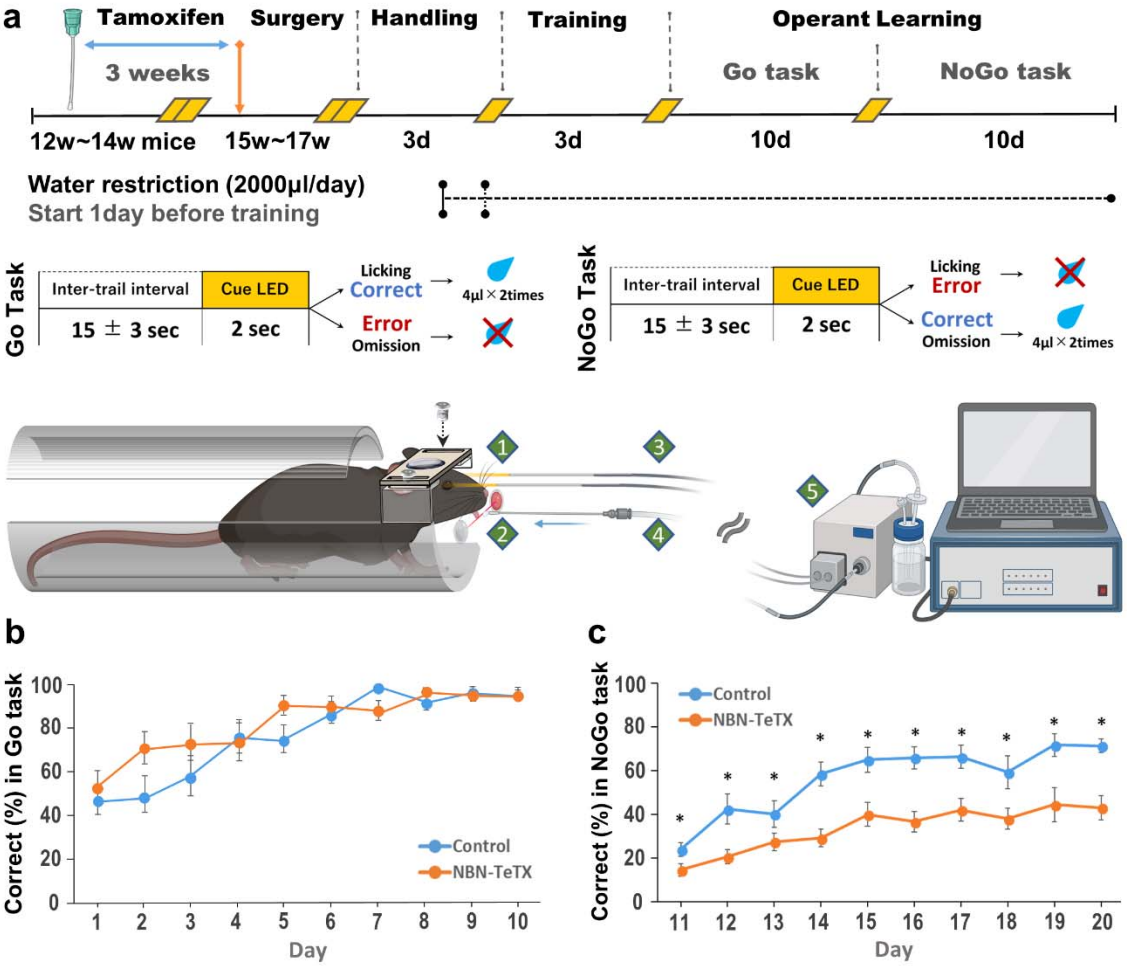

Figure 4. Inhibiting newborn neuron function impairs inhibitory control and induces compulsive behavior.

a. After 3 weeks of receiving tamoxifen injections in 3- to 4-month-old NBN-TeTX mice and controls, surgical manipulation of the head immobilization device was performed. Postoperative rest was given for 1 day. And a 3-day handling was conducted. The maximum water intake of the mice was restricted to 2000 μL per day starting on the last day of handling and continued until the end of the experiment. A 3-day light-cued water licking training was conducted following the end of the handling. Individuals that completed the training well (NBN-TeTX: n=11, Ctrl: n=9) were entered into subsequent Go task and Nogo task experiments of 10 days each.

b. The trend of the correct rate of each group during the 10-day Go task was shown. By day 10, both groups had achieved a correct rate of 95% or higher for two consecutive days, and there was no significant difference in the correct rate between the two groups. (Go task: day 9 correct rate: NBN-TeTX: 94.96%, Ctrl: 96.37%, genotype × day interaction: $F(9, 162) = 1.0921$, $p = 0.3714$; day10 correct rate: NBN-TeTX: 95.68%, Ctrl: 95.72%, genotype: $F(1, 18) = 0.9056$, $p = 0.3539$, two-way repeated measures ANOVA with Bonferroni post hoc test.)

c. The results of the 10-day Nogo task showed a major effect of genotype on the correct licking rate. The NBN-TeTX group lagged behind the control group throughout the entire task, and the correct rate remained below 40% until the end of the experiment. (Nogo task: genotype: $F(1, 18) = 16.6545$, $p = 0.0007$, $^*p<0.05$, two-way repeated measures ANOVA with Bonferroni post hoc test.)

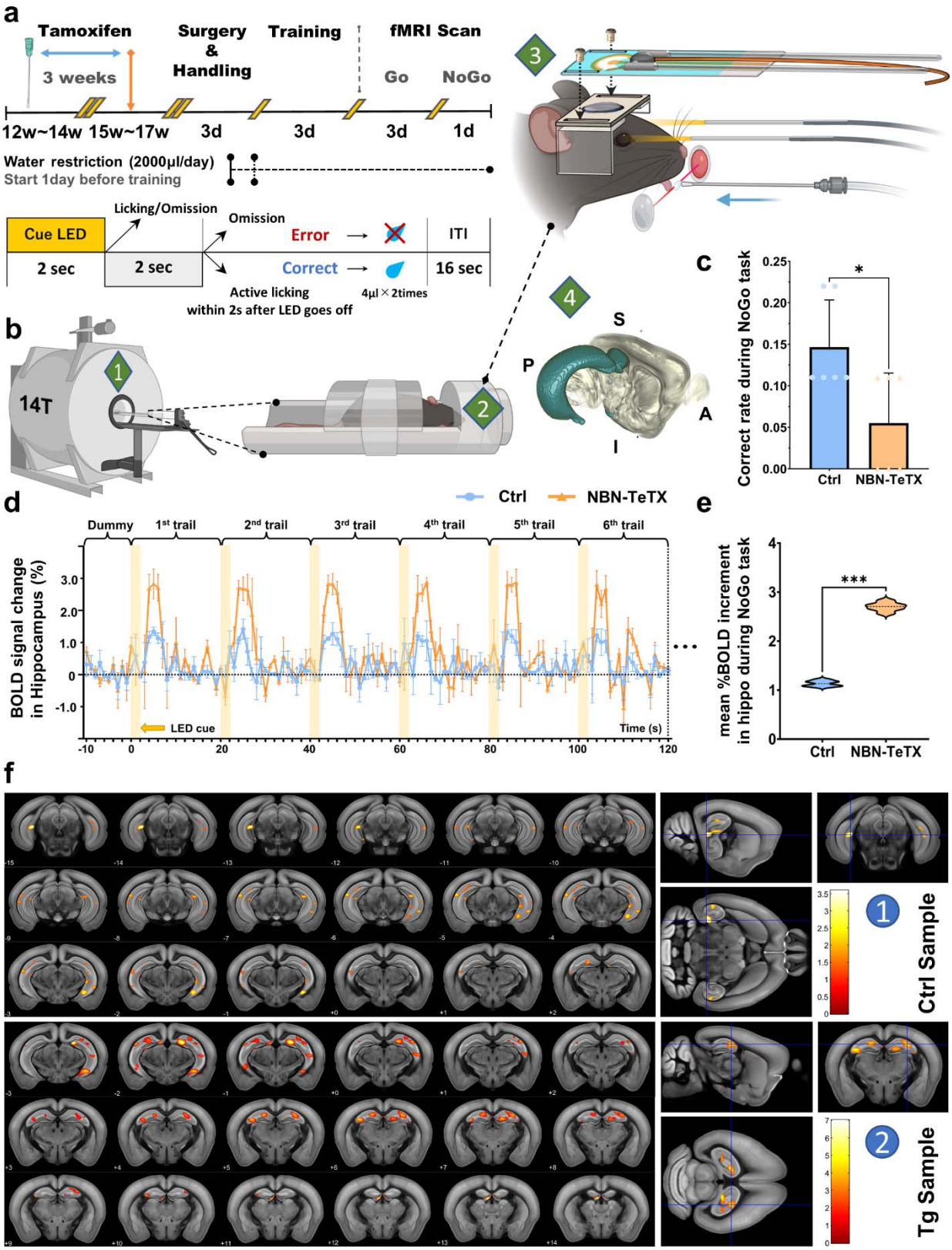

Figure 5. Silencing of newborn neurons triggers abnormally elevated hippocampal activity in reversal learning

a. Schematic diagram and protocol for a light-cued operant learning experiment of water licking combined with fMRI scanning. Unlike the previous operant learning experiments, in the Nogo task, in order to avoid the mice directly receiving the water reward due to omission, we changed the rule to require active licking within two seconds after the end of the light cue in order to be considered correct and receive the water reward. To prevent the hemodynamic response function overlap, we fixed one trail for 20s, the first 2s for light cueing, followed by 2s of judgment waiting time and 16s of fixed inter-trail interval time. The task-based fMRI lasted for a total of 3 min, during which 9 trails were included.

b. A custom-made animal fixation bed (mark 2) containing light stimulation, infrared sensors and water administration devices (mark 3) was used to perform scans in a 14T fMRI equipment (marker 1). The data were analyzed using the hippocampal region based on the Allen mouse atlas as the voxel of interest (VOI) (mark 4).

c. Comparison of the correct licking rate of the two groups in 9 NoGo tasks during formal scanning. The Tg group significantly lagged behind the Ctrl group. (NBN-TeTX: n=6, Ctrl: n=6, *$p < 0.05$; student's t-test)

d. Shows the percentage change in hippocampal BOLD signal in the Nogo task of Ctrl and NBN-TeTX groups (the first 6 of 9 trials). The percent BOLD signal change of the hippocampus was consistently higher in the Tg group than in the Ctrl group between 4-6 s after the start of each trial.

e. Comparing the mean %BOLD change between 4-6s in each trial to their baseline, the results showed that the NBN-TeTX group had approximately 2.45 times more %BOLD rise in reversal learning than the Ctrl group (NBN-TeTX: n=6, Ctrl: n=6, mean %BOLD change: Ctrl: 1.13±0.058, Tg: 2.70±0.089, ***$p < 0.001$, student's t-test).

e. The above shows the results of representative Ctrl individuals analyzed at 1st-level. No significant differences were found at set-level, cluster-level, and peak-level. Images were drawn under pFDR-corr<0.05, threshold k=7; scale bar represents T-score, height threshold T=2.351464. The coordinates show the global maximum value at [-28mm, -15mm, -4mm]. The lower part shows the results of the representative Tg individuals at 1st-level analysis. At the peak level, a small number of voxels with significant differences were detected. Images were drawn under pFDR-corr<0.05, threshold k=7; height threshold T=3.145452. The coordinates show the global maximum value at [-20mm, 6mm,13mm].

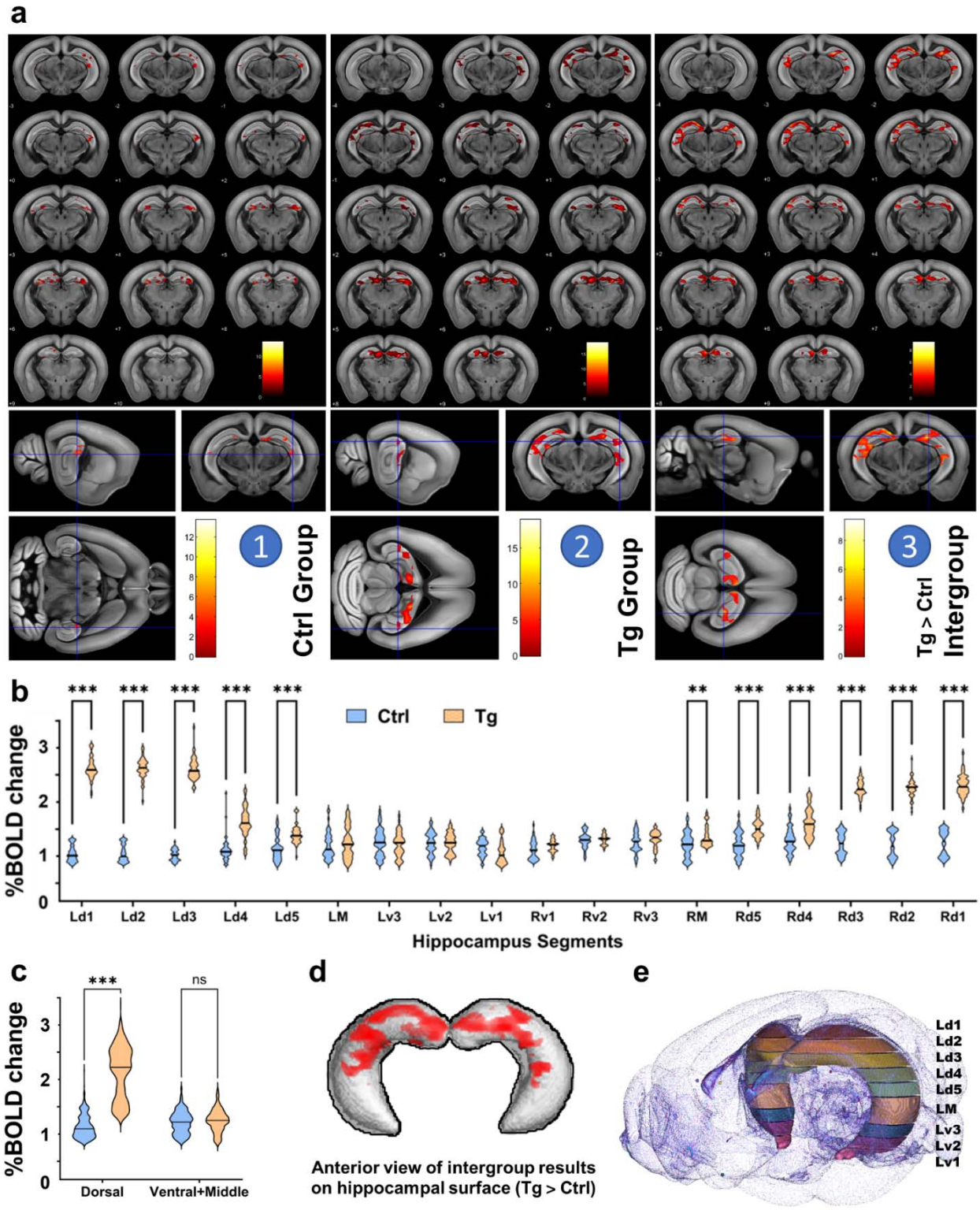

Figure 6. The activation heterogeneity induced by silencing newborn neurons along hippocampal longitudinal axis.

a. Shows the results of 2nd-level analysis of hippocampus activity for each group during the Nogo task at about 5s (4-6s) after the start of light stimulus (0-2s) compared to the baseline. One the left, the results of intragroup for Ctrl group is shown. Images were drawn under pFDR-corr<0.05, threshold k=7; scale bar represents T-score, height threshold T=2.552380. The coordinates show the global maximum value at [29mm, -2.5mm, -2mm], kE=2303. The middle parts show the intragroup results of Tg group. Images were drawn under pFDR-corr<0.05, threshold k=7; height threshold T=2.718079. The coordinates show the global maximum value at [19mm, 4.5mm, 9mm], kE=3414. The right parts show the intergroup differences for Tg > Ctrl. Images were drawn under pFDR-corr<0.05, threshold k=7; height threshold T=2.602480. The coordinates show the global maximum value at [20mm, -2mm, 12mm], kE=9089.
b. Shows the comparison of hippocampal %BOLD change along the longitudinal axis from dorsal to ventral in the two groups during Nogo task. The results showed that the abnormal increased hippocampal activity shown in the NBN-TeTX group was mainly contributed by the dorsal hippocampus. This abnormal rise gradually decreases along the longitudinal axis of the hippocampus from dorsal to ventral and no longer shows significant differences from approximately the middle. (NBN-TeTX: n=6, Ctrl: n=6, ***p < 0.001, **p < 0.01, two-way repeated measures ANOVA with Bonferroni post hoc test.)
c. Comparisons of the dorsal hippocampus with the ventral hippocampus were performed by pooling the segments, and the results showed that NBN-TeTX had a significant difference in activity only in the dorsal hippocampus compared to the control group, while the ventral hippocampus was almost identical. (NBN-TeTX: n=6, Ctrl: n=6, ***p < 0.001, two-way repeated measures ANOVA with Bonferroni post hoc test.)
d. Projection of the results of second-level intergroup analysis on the hippocampal surface. Highly activated regions with significant differences were mainly distributed in the dorsal hippocampus.
e. Schematics of the hippocampal segmentation used in the above analysis are shown. In the results figure 5b, the hippocampal region was divided equally into 10 parts as masks based on Allen mouse atlas. The uppermost five parts were considered the dorsal hippocampus, the middle two were considered the middle, and the lowermost three were considered the ventral hippocampus. While in the results figure 5c, the middle and ventral parts were grouped together for comparison with the dorsal hippocampus.

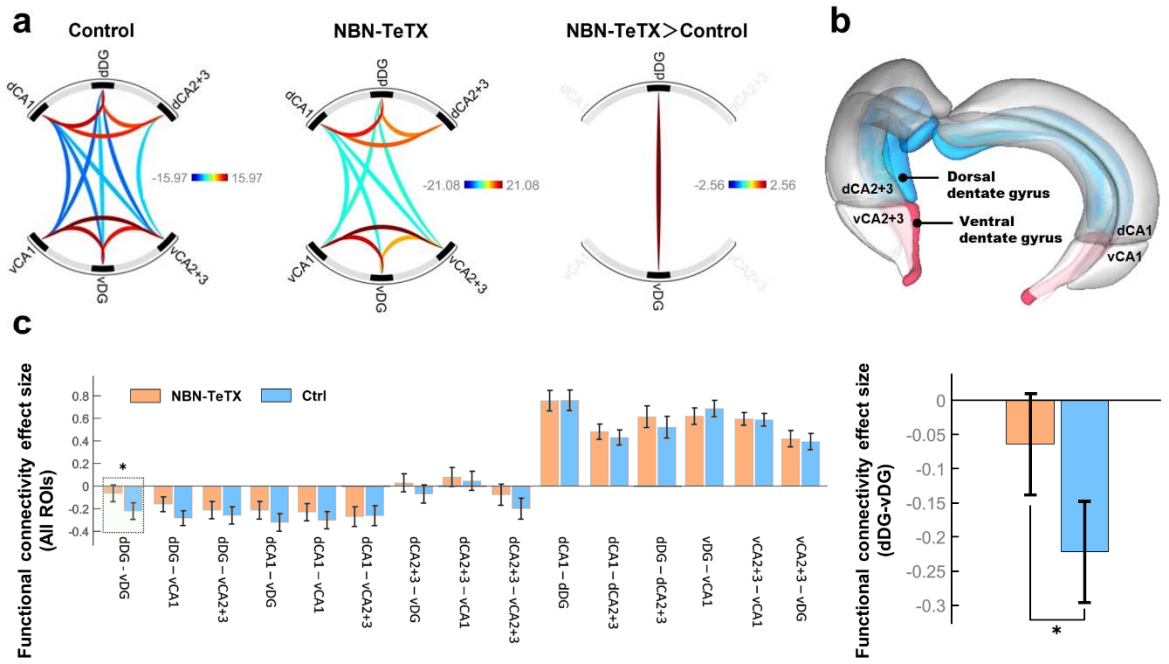

Figure 7. Silencing of newborn neurons induces enhanced functional connectivity between the dorsal dentate gyrus and ventral dentate gyrus

a. Shows the intragroup functional connectivity connectome ring within the hippocampus of the Control and NBN-TeTX groups in resting-state fMRI analysis, and the structures with significant differences under NBN-TeTX>Ctrl. The results showed that silencing the newborn neurons enhanced the functional connectivity between the dorsal and ventral hippocampus, specifically, causing a negative functional correlation of attenuation. (NBN-TeTX: n=14, Ctrl: n=14, intragroup images were drawn under connection threshold: $p<0.05$, p-FDR corrected; cluster threshold $p<0.05$, cluster-level p-FDR corrected (MVPA omnibus test), two-sided; intergroup images were drawn under connection threshold: $p<0.05$, p-FDR corrected.)

b. Anatomical structure-based masking was used in the analysis of rs-fMRI. The dentate gyrus, CA1 and CA2+3 was divided into dorsal (upper 7/10) and ventral (lower 3/10), for a total of 6 ROIs.

c. The left shows a comparison of the functional connectivity effect size (Fisher-transformed z-values) among the entire hippocampal internal components between the NBN-TeTX and Ctrl groups under resting state, while the right shows the difference effect size between the dorsal dentate gyrus and ventral gyrus under the above analyzed conditions. (NBN-TeTX: n=14, Ctrl: n=14, beta=0.16, T(26)=2.56, *p=0.016, student's t-test.)

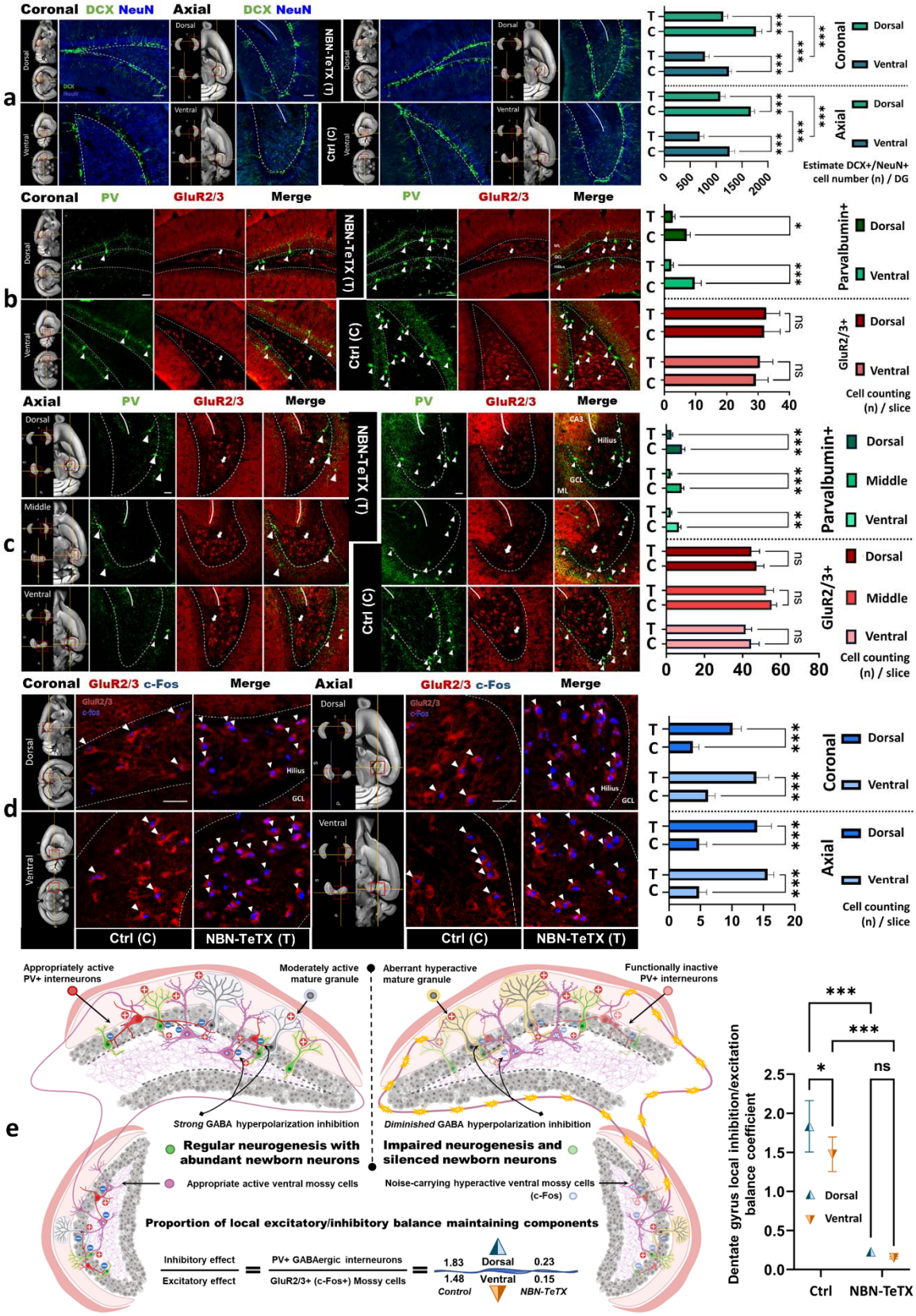

Figure 8. The role of newborn neurons in the dentate gyrus longitudinal coordination of PV+ interneurons and mossy cells

a. Immature newborn neurons were counted separately in the dorsal and ventral hippocampus (Simultaneous use of coronal and axial slices). In comparison to the control group, the NBN-TeTX group demonstrated a significant loss of immature newborn neurons three weeks after tamoxifen injection. Furthermore, compared to the ventral side, the dorsal side contained significantly more newborn neurons in both groups. (DCX+/NeuN+: NBN-TeTX: n=6, Ctrl: n=6, ***$p < 0.001$, two-way repeated measures ANOVA with Bonferroni post hoc test, scale bar=100μm.)

b. Immunofluorescence staining of GABAergic interneurons represented by PV+ cells and mossy cells represented by Glu2/3 performed in the dorsal and ventral sides of the hippocampal dentate gyrus, respectively (upper: dorsal, lower: ventral, coronal slices). The results showed that the number of PV+ expressing interneurons in the NBN-TeTX group was significantly downregulated both dorsally and ventrally in the hippocampus, but this change did not differ between the dorsal and ventral sides. Moss cells, on the other hand, showed no significant difference in the number of fluorescent expressions. (PV+: NBN-TeTX: n=6, Ctrl: n=6, *$p < 0.05$, one-way repeated measures ANOVA with Bonferroni post hoc test, scale bar=100μm.)

c. Changes in the number of fluorescently expressing cells in the longitudinal axis of the hippocampus were confirmed by staining the dorsal (upper), middle and ventral (lower) dentate gyrus segments separately (axial slices). The results showed that PV+ interneurons were significantly reduced throughout the longitudinal axis, and again, the reduction did not show differences among the three segments. In contrast, mossy cells did not show significant differences in any of the three parts. (PV+: NBN-TeTX: n=6, Ctrl: n=6, ***$p < 0.001$, ** $p < 0.01$, one-way repeated measures ANOVA with Bonferroni post hoc test, scale bar=100μm.)

d. Shows the results of GluR2/3 and c-Fos co-fluorescence staining of the dorsal and ventral hippocampal dentate gyrus in coronal sections and axial sections, respectively. The results showed that the expression of c-Fos was significantly higher in both dorsal and ventral dentate gyrus mossy cells in the NBN-TeTX group. In addition, this elevation did not differ dorsoventrally. (NBN-TeTX: n=6, Ctrl: n=6, ***$p < 0.001$, ** $p < 0.01$, two-way repeated measures ANOVA with Bonferroni post hoc test, scale bar=50μm.)

e. A schematic representation of the mechanisms involved in the regulation of excitation/inhibition homeostasis in the hippocampal dentate gyrus by 2-5-week-old newborn neurons (NBNs). When NBNs are functionally silenced or deficient due to insufficient neurogenesis, their sparse projections to inhibitory interneurons localized to the hippocampal dentate gyrus are also impaired as a result. These dentate gyrus localized PV+ interneurons may be functionally downregulated or reduced in number due to a lack of stimulatory signals from highly excitatory NBNs, leaving abnormally local neuronal activity upregulation due to a lack of inhibitory signals. On the other hand, the primary inhibitory function of local mossy cells through stimulation of GABAergic interneurons shifts to a direct activating function on newborn neurons and granule cells, which show excessive excitation due to the lack of inhibition by GABAergic neurons, resulting in an intensified upregulation of "activity noise" in the dentate gyrus. When these highly activated neurons reach a certain level, they may alter functional connectivity within the hippocampus, affecting the functional heterogeneity of the dorsoventral hippocampus and leading to impaired hippocampus-dependent learning and memory functions and ultimately affecting higher cognitive functions, including cognitive flexibility. Besides, the inhibitory coefficient of the dentate gyrus is greater than the excitatory coefficient in general, and it is more pronounced dorsally. When newborn neurons are silenced, the overall inhibitory coefficient of the dentate gyrus drops dramatically, and the dorsal side loses its inhibitory

advantage in comparison to the ventral side. This may alter the normal dorsoventral excitatory-inhibitory component relationship, leading to more prominent dorsally located abnormal hyperactivation.

Gene Name	Primer sequences Reaction system composition & Reaction conditions
Tg1 Nestin-CreERT2 (~340 bp)	**Primer sequences** 5'-TTCCGCTGGGTCACTGTCGCCGCTAC-3' (Fw) 5'-TAATCGCGAACATCTTCAGGTTCTGC-3' (Rv) **Reaction system composition** Template DNA (DNA solution) 1 μL 10 × PCR buffer 10 fold dilution dNTP mixture 0.2 mM Primer (Fw/Rv) 0.4 μM each Internal control primer 0.4 μM each Taq 0.3 units DDW up to 15 μL **Reaction condition** 95℃ 1 min.; 94℃ 30 sec., 53℃ 45 sec., 72℃ 1 min., × 32 cycles; 72℃ 5 min.
Tg2 αCamKII promoter-loxP-STOP-loxP-tTA (~500 bp)	**Primer sequences** 5'-CGCTGTGGGGCATTTTACTTTAG-3' (Fw) 5'-GGGTCCATGGTGATACAAGG-3' (Rv) **Reaction system composition** Template DNA (DNA solution) 1 μL 10 × PCR buffer 10 fold dilution dNTP mixture 0.2 mM Primer (Fw/Rv) 1.0 μM each Internal control primer 0.5 μM each Taq 0.45 units DDW up to 15 μL **Reaction condition** 94℃ 3 min.; 94℃ 30 sec., 60℃ 30 sec., 72℃ 30 sec., × 35 cycles; 72℃ 2 min.
Tg3 Tet Operator-TeTX (173 bp)	**Primer sequences** 5'-AAGTTCATCTGCACCACCG-3' (Fw) 5'-TCCTTGAAGAAGATGGTGCG-3' (Rv) **Reaction system composition** Template DNA (DNA solution) 1 μL 10 × PCR buffer 10 fold dilution dNTP mixture 0.2 mM Primer (Fw/Rv) 0.5 μM each Internal control primer 0.5 μM each Taq 0.45 units DDW up to 15 μL **Reaction condition** 95℃ 1 min.; 94℃ 20 sec., Touch down over (internal temp. 65℃, Final temp. 60℃) 15 sec., 68℃ 10 sec. × 10 cycles; 94℃ 15 sec., 60℃ 15 sec., 72℃ 10 sec., × 28 cycles; 72℃ 2 min.
Internal positive control primer (for Tg1) (550 bp)	**Primer sequences** 5'-GTTAGCATTGAGCTGCAAGCGCCGTCT-3' (Fw) 5'-TGAGCGAGCTCATCAAGATAATCAGGT-3' (Rv)
Internal positive control primer (for Tg2, Tg3) (324 bp)	**Primer sequences** 5'-CTAGGCCACAGAATTGAAAGATCT-3' (Fw) 5'-GTAGGTGGAAATTCTAGCATCATCC-3' (Rv)

Figure S1. Gene sequence of NBN-TeTX transgenic mice